NASA TECHNICAL NOTE

NASA TN D-6623

MAGNETOSTRICTION AND MAGNETOELASTIC QUANTUM OSCILLATIONS IN p-TYPE LEAD TELLURIDE

by T. E. Thompson, Paul R. Aron, B. S. Chandrasekhar, and D. N. Langenberg

Lewis Research Center
Cleveland, Ohio 44135

NATIONAL AERONAUTICS AND SPACE ADMINISTRATION • WASHINGTON, D. C. • JANUARY 1972

1. Report No. NASA TN D-6623	2. Government Accession No.	3. Recipient's Catalog No.
4. Title and Subtitle MAGNETOSTRICTION AND MAGNETOELASTIC QUANTUM OSCILLATIONS IN p-TYPE LEAD TELLURIDE		5. Report Date January 1972 6. Performing Organization Code
7. Author(s) T. E. Thompson, Paul R. Aron, B. S. Chandrasekhar, and D. N. Langenberg (see p. ii for authors' affiliation)		8. Performing Organization Report No. E-6524 10. Work Unit No. 112-02
9. Performing Organization Name and Address Lewis Research Center National Aeronautics and Space Administration Cleveland, Ohio 44135		11. Contract or Grant No. 13. Type of Report and Period Covered Technical Note
12. Sponsoring Agency Name and Address National Aeronautics and Space Administration Washington, D. C. 20546		14. Sponsoring Agency Code

15. Supplementary Notes

16. Abstract

A detailed experimental and theoretical study of quantum oscillations in the magnetostriction and Young's modulus of p-PbTe is presented. The valance band of PbTe is approximated by a spheroidal, nonparabolic model in which the effects of strain on the valance band parameters are described by a deformation potential model. Using appropriate thermodynamic derivatives of the modified Lifshitz-Kosevich expression for the oscillatory parts of the electronic free energy, it is shown that both types of oscillations arise mainly from relative shifts of the valance band maxima due to shear strains, accompanied by intervalley charge transfer. Band parameters derived from the periods, phases, and spin splitting of the oscillations are in generally good agreement with values reported by other workers. A detailed comparison is made of the experimentally observed oscillation amplitudes with those predicted by theory, and satisfactory agreement is found. The ratio of the amplitudes of the two effects yields a value of the valence band deformation potential, $\Xi_u^V = 7.9 \pm 1.3$ eV, in good agreement with a value found from piezoresistance experiments by Burke.

17. Key Words (Suggested by Author(s)) 	18. Distribution Statement Unclassified - unlimited		
19. Security Classif. (of this report) Unclassified	20. Security Classif. (of this page) Unclassified	21. No. of Pages 48	22. Price* $3.00

* For sale by the National Technical Information Service, Springfield, Virginia 22151

Authors: T. E. Thompson, University of Pennsylvania, Philadelphia, Pennsylvania; Paul R. Aron, Lewis Research Center; B. S. Chandrasekhar, Case Western Reserve University, Cleveland, Ohio; D. N. Langenberg, University of Pennsylvania, Philadelphia, Pennsylvania.

MAGNETOSTRICTION AND MAGNETOELASTIC QUANTUM OSCILLATIONS IN p-TYPE LEAD TELLURIDE*

by T. E. Thompson,† Paul R. Aron, B. S. Chandrasekhar,‡ and D. N. Langenberg**

Lewis Research Center

SUMMARY

A detailed experimental and theoretical study of quantum oscillations in the magnetostriction and Young's modulus of p-type lead telluride is presented. The valance band of lead telluride is approximated by a spheroidal, nonparabolic model in which the effects of strain on the valance band parameters are described by a deformation potential model. Using appropriate thermodynamic derivatives of the modified Lifshitz-Kosevich expression for the oscillatory parts of the electronic free energy, it is shown that both types of oscillations arise mainly from relative shifts of the valance band maxima due to shear strains, accompanied by intervalley charge transfer. Band parameters derived from the periods, phases, and spin splitting of the oscillations are in generally good agreement with values reported by other workers. A detailed comparison is made of the experimentally observed oscillation amplitudes with those predicted by theory, and satisfactory agreement is found. The ratio of the amplitudes of the two effects yields a value of the valance band deformation potential, $\Xi_u^V = 7.9 \pm 1.3$ eV, in good agreement with a value found from piezoresistance experiments by Burke.

INTRODUCTION

The Landau quantization of the energy levels of the conduction electrons in a solid placed in a magnetic field forms the basis for some of the most powerful techniques for establishing the electronic structure of solids (ref. 1). One can construct, using the thermodynamic potential for the electronic system as calculated by Lifshitz and Kosevich (ref. 2), a free energy which is a function of the magnetic field, the tempera-

*Work supported in part by the Advanced Research Projects Agency and the U. S. Air Force Office of Scientific Research, Office of Aerospace Research.

†Assistant Professor of Electrical Engineering, University of Pennsylvania, Philadelphia, Pennsylvania.

‡Professor of Physics, Case Western Reserve University, Cleveland, Ohio.

**Professor of Physics, University of Pennsylvania, Philadelphia, Pennsylvania.

ture, and the elastic strain. The first derivatives of the free energy with respect to these three thermodynamic variables lead, respectively, to the magnetization, the entropy, and the elastic stress. Because of the quantization of the electronic states, the free energy is periodic in the reciprocal of the magnetic field. This oscillatory character is consequently manifest in the magnetization, entropy, and stress.

The oscillatory magnetization (de Haas-van Alphen effect) has been most extensively used in the study of Fermi surfaces in metals. More recently, the oscillatory entropy, which is revaled as temperature oscillations in a thermally isolated crystal subjected to a swept magnetic field, has also been developed as a useful tool for such studies. The third effect, which appears as an oscillatory magnetostriction (i.e., the dimensional change of a crystal placed in a magnetic field), forms one of the subjects of this paper. The elastic constants of the crystal, which are the second derivatives of the free energy with respect to strain, also show quantum oscillations, and form the second main topic of this paper.

We have measured the oscillatory behavior of the magnetostriction and the Young's modulus of single crystals of p-type lead telluride, a multivalley, degenerate semiconductor, and determined from these results the periods, phases, effective masses, and g-factors for this material. From the amplitudes of these two effects we have also determined the deformation potential Ξ_u^V for the valance band in lead telluride. The amplitude analysis is considerably simplified by using the ratio of the amplitudes of the two effects. This method of obtaining deformation potentials in semiconductors, or the generalized deformation parameters for Fermi surfaces in metals, is a new and important feature of the techniques described in this paper.

Magnetostriction (MS) was first observed by Joule in 1842 in a bar of iron (ref. 3). The main body of work since that time has been on ferromagnetic materials in which the effect is largest: the strains in iron and nickel are typically 10^{-5} to 10^{-6} at the saturation field. The first observation of MS in a nonferromagnetic material was made by Kapitza in 1929 in a series of classic experiments in pulsed fields up to 250 kG (ref. 4). Kapitza observed a monotonic MS in bismuth, antimony, graphite, gallium, tin, and tungsten, finding the effect to be greatest in bismuth, where the strain ϵ is $\sim 10^{-5}$ in a field of 15 tesla (150 kG) at room temperature.

In 1963, Chandrasekhar pointed out that oscillatory MS should be observable in materials that show the de Haas-van Alphen effect (ref. 5). Subsequently, Green and Chandrasekhar observed the first such oscillations in bismuth (ref. 6). Magnetostriction oscillations have since been observed in silver (ref. 7), arsenic (ref. 8), beryllium (ref. 9), bismuth (ref. 10), cadmium (ref. 11), chromium (ref. 12), copper (refs. 13 and 6), gallium (P.A. Pentz private communication), gallium antimonide (ref. 14), lead telluride (refs. 15 and 16), antimony (ref. 17), lead (ref. 12 and private communications from M. M. Finkelstein and from A. J. Slavin), and zinc (ref. 18). One of us (P.R.A.,

unpublished) has observed MS oscillations in gold. The oscillatory strain amplitudes for these materials at 2.5 tesla (25 kG) and temperatures near 4 K range between 10^{-6} and 10^{-9}. For lead telluride at this temperature and field, $\epsilon \sim 10^{-7}$.

Magnetostriction in diamagnetic systems is related directly to the strain dependence of the Fermi surface. Shoenberg (see ref. 14) was one of the first to point out that the diamagnetic oscillatory magnetostriction could be analyzed in terms of the oscillatory magnetization M and the strain dependence of the appropriate extremal cross-sectional area of the Fermi surface:

$$\epsilon_i = -MB\, s^o_{ij} \frac{\partial \ln S_m}{\partial \epsilon_j} \tag{1}$$

where B is the magnetic field, s^o_{ij} is a component of the elastic compliance tensor, and S_m is the extremal cross-sectional area of the Fermi surface perpendicular to the applied magnetic field. (Throughout this report we use the standard "engineering" form of the reduced stress and strain tensors (ref. 19).) Equation (1) was derived using thermodynamic considerations together with the assumption that the strain dependence of the oscillatory diamagnetic free energy is dominated by the strain dependence of the S_m which appears in the argument of the oscillatory factor in the free energy (see eq. (16)). The gallium antimonide and beryllium experiments were analyzed using equation (1); a value for $\partial \ln S_m/\partial \epsilon_j$ was found by measuring separately the magnetization and magnetostriction oscillations. In the present report we derive an expression for the magnetostriction in terms of $\partial \ln S_m/\partial \epsilon_j$ directly from the total free energy, using a modified form of the Lifshitz-Kosevich expression for the diamagnetic free energy. We then use a simple multivalley, deformation potential model to relate $\partial \ln S_m/\partial \epsilon_j$ to the strain dependence of the lead telluride valance band. A similar method has been used by Aron and Chandrasekhar for bismuth (ref. 10) and by the Naval Ordnance Laboratory group for lead telluride (ref. 16). However, the results and conclusions in reference 16 differ from ours at several points. An important new aspect of our analysis is the direct comparison of the MS oscillations with quantum oscillations in the elastic constant (ref. 20). We call these magnetoelastic (ME) oscillations to distinguish them from sound velocity oscillations which have also been observed (ref. 21). By taking the ratio of the amplitudes of these two effects, the analysis is considerably simplified in a manner similar to the simplification obtained by taking the ratio of the amplitudes of the MS oscillations and the magnetization oscillations in equation (1).

Rodriguez (refs. 22 and 23) derived an expression for the velocity oscillations by considering the electronic contribution to the bulk modulus. He simply calculated the second derivative with respect to volume of the Lifshitz-Kosevich expression for the diamagnetic free energy of a free-electron gas, assuming the major contribution to this

derivative to come from the strain dependence of the S_m, which appears in the oscillatory factor, and using the free-electron expression $\partial \ln S_m/\partial V = -2/3$. This approach is quite similar to those mentioned in the preceding section for calculating expressions for the MS oscillations. For the analysis of their beryllium experiments, Testardi and Condon (ref. 24) derived expressions relating elastic constant oscillations to magnetization oscillations. They measured separately the magnetization and velocity oscillations and from the combined data report values of $\partial \ln S_m/\partial \epsilon_j$. The ideas behind their arguments are quite similar to those used to derive equation (1), where the magnetization and ME oscillations are related. Whereas Rodriguez's equations are limited to the free-electron gas, a ratio method such as that used by Testardi and Condon can be applied to an electronic system with a more general Fermi surface. Testardi and Condon also included B-H effects and the interaction between ϵ and B in their analysis.

In this report, we describe a spheroidal, nonparabolic, multivalley, deformation potential model of the valance band of lead telluride. We derive theoretical expressions in terms of our valance band model for the MS and ME oscillations from the appropriate strain derivatives of a modified form of the Lifshitz-Kosevich free energy. Band parameters obtained from the experimental results are compared with results previously obtained by other workers. An analysis of the amplitudes of the MS and ME oscillations and their ratio is presented, leading to an experimental value of the valance band deformation potential Ξ_u^v for PbTe. Some basic relations for the spheroidal, nonparabolic energy-band model are presented in the appendix.

LEAD TELLURIDE VALANCE BAND

Lead telluride (PbTe) is a cubic (NaCl structure, point group m3m) degenerate semiconductor characterized (at liquid-helium temperatures) by a small energy gap (~0.2 eV), high carrier mobilities $\gtrsim 10^5$ cm^2 v^{-1} sec^{-1}), and small effective masses (~0.05 m_o). A mass of experimental evidence (de Haas-van Alphen oscillations, Shubnikov-de Haas oscillations, Azbel-Kaner cyclotron resonance, interband magneto-optical absorption, and other optical and transport phenomena (see references in the beginning of ref. 25)) indicates that the Fermi surface of both p- and n-type PbTe is well described by ⟨111⟩ directed prolate spheroids centered on the L-points of the Brillouin zone (fig. 1). There are eight half-spheroids or, equivalently, four full spheroids in the zone.

Cuff, Ellett, and Kuglin (refs. 26 and 27) found a strong carrier concentration dependence of the ⟨111⟩ cyclotron mass for p-type PbTe, which indicates that the valance band of this material is nonparabolic. Dixon and Riedl (ref. 28) found similar results for the carrier concentration dependence of the electric-susceptibility hole mass of PbTe. In order to take nonparabolicity into account we use a model due largely to Kane

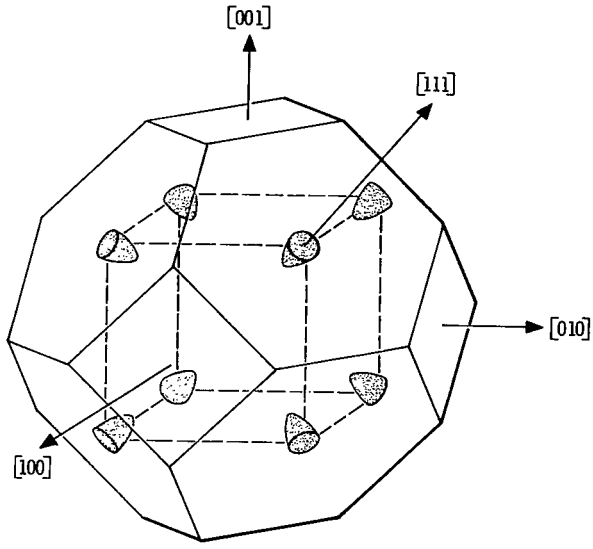

Figure 1. - The Brillouin zone of lead telluride showing the eight, ⟨111⟩- directed, half-spheroids that contain the carriers (either electrons or holes).

(ref. 29) and Cohen (ref. 30). Considering the symmetry of PbTe and using a coordinate system where p_3 is the momentum component along [111], and p_1 and p_2 are the two orthogonal components, Cohen's equation (26) becomes

$$\frac{p_1^2 + p_2^2}{2m_1} = \left(E - \frac{p_3^2}{2m_3} \right) \left(1 + \frac{E}{E_g} + \frac{p_3^2}{2E_g m_3'} \right) \tag{2}$$

where E_g is an effective energy gap between the valance and conduction bands, m_1 and m_3 are the band edge effective masses, and m_3' is the longitudinal effective mass of the conduction band, which is experimentally found to be of the same order of magnitude as m_3 (ref. 31). The Fermi surface is more easily visualized by writing equation (2) in the form

$$E = \frac{p_1^2 + p_2^2}{2m_t} + \frac{p_3^2}{2m\ell} \tag{3}$$

where

$$m_t = m_1 \left(1 + \frac{E}{E_g} + \frac{p_3^2}{2E_g m_3'} \right) \tag{4}$$

and

$$m_\ell = m_3 \tag{5}$$

Equation (3) describes a surface of revolution about the 3-axis, which has extremal cross sections at $p_3 = 0$ and $p_3^2 = m_3' E_g \left[(E/E_g)(m_3/m_3' - 1) - 1 \right]$. For the energy and mass values of our samples the second extremum does not exist, and the Fermi surface is spheroidal except for a slight bulging for large values of p_3. In this connection, we note that recent work by Schilz (ref. 32) indicates that when the carrier concentration becomes large ($p > 5 \times 10^{18}$ cm^{-3}), the valance band Fermi surface becomes cylindrical in shape. The extremal cross section perpendicular to the p_3 axis, located at $p_3 = 0$, is given by

$$S_{m3} = 2\pi m_1 E \left(1 + \frac{E}{E_g} \right) \tag{6}$$

The cyclotron orbits of importance in the present work do not traverse large values of p_3, so that the p_3 dependence of the transverse mass indicated in equation (4) is small and can be neglected. Instead of equation (4) we therefore use

$$m_t = m_1 \left(1 + \frac{E}{E_g} \right) \tag{7}$$

Equations (3), (5), and (6) describe the spheroidal, nonparabolic model for the energy surfaces of p-type PbTe, which we use throughout the remainder of this report. As is conventional, we also define a mass anisotropy parameter $K = m_\ell / m_t$, which in our model has an energy dependence of the form $K = (m_3/m_1)\left[1 + (E/E_g) \right]^{-1}$.

A test of the validity of the model and an evaluation of the numerical values of the model parameters appropriate to p-PbTe can be made using our data and the data of Cuff, Ellett, and Kuglin (ref. 26). When the magnetic field is parallel to the unique axis

of the spheroid, the quantum oscillation period P_3 is given by

$$P_3 \equiv \frac{eh}{cS_{m3}} = \frac{e\hbar}{cE_F m_1 \left(1 + \frac{E_F}{E_g}\right)} \tag{8}$$

and the corresponding normalized cyclotron mass μ_3 is

$$\mu_3 \equiv \frac{1}{2\pi m_o} \frac{\partial S_{m3}}{\partial E}\bigg|_{E=E_F} = \frac{m_1}{m_o}\left(1 + 2\frac{E_F}{E_g}\right) \tag{9}$$

(For derivations of these relations, see the appendix. In this report μ is always used to denote cyclotron masses normalized to m_o, the free electron mass, and m is always used to denote unnormalized band masses. Notice that $\mu_3 m_o \neq m_t$.) Solving for E_F from equation (8), substituting this value of E_F into equation (9), and squaring the result give the relation

$$\mu_t^2 = \left(\frac{m_1}{m_o}\right)^2 + Cm_1(P_3 E_g m_o)^{-1} \tag{10}$$

where $C = 4\, e\hbar/(m_o c) = 4.63\times10^{-4}$ electron volt per tesla. Thus, a plot of μ_t^2 against P_3^{-1} gives the band edge mass m_1 and the energy gap E_g. Such an analysis was carried out in reference 27, and in figure 2 shows a plot of their data along with values found from this experiment. A least-squares fit of the data gives $m_1 = (0.018\pm0.003)\, m_o$ and $E_g = 0.10\pm0.02$ electron volt. Cuff, Ellett, Kuglin, and Williams (ref. 27) find a different value for m_1. This discrepancy appears to originate from the fact that their equation (2) is not equivalent to our equation (10), although it appears that the same model is being considered. A similar study indicates that m_l is essentially constant over the range of carrier concentrations 3.6×10^{17} per cubic centimeter $< p < 3.5\times10^{18}$ per cubic centimeter and has a value $m_l = m_3 = (0.10\pm0.02)\, m_o$.

The direct gap Δ between the valance and conduction bands of PbTe at $T = 4.2$ K has been determined in two different experiments. Mitchell, Palik, and Zemel (ref. 33) find $\Delta = 0.190\pm0.002$ electron volt from magneto-optical studies of epitaxial films and Butler and Calawa (ref. 34) find $\Delta = 0.187$ electron volt from magneto-emission studies with PbTe diode lasers. The fact that the effective gap E_g in our model is smaller than the measured direct optical gap Δ indicates that interactions between the valence band

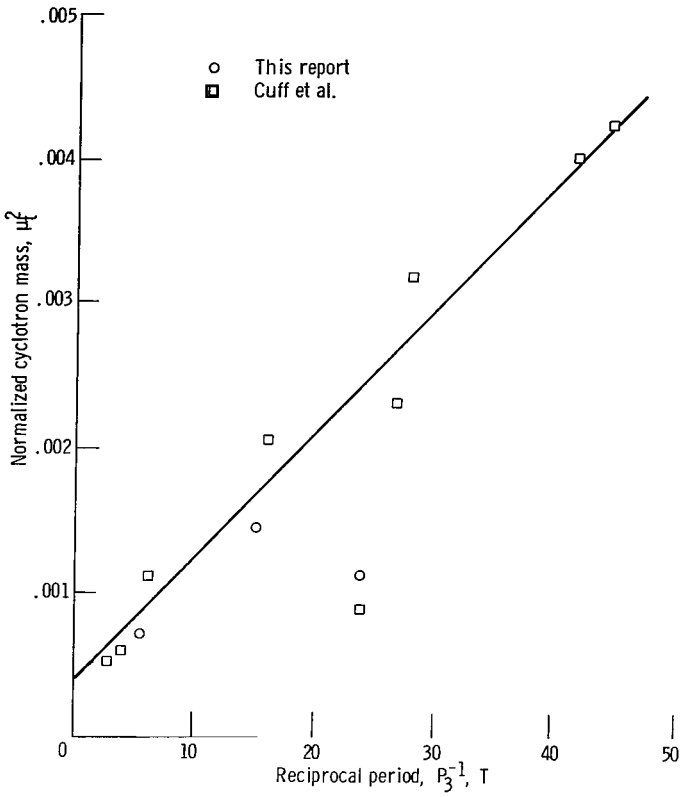

Figure 2. - Square of normalized cyclotron mass plotted against reciprocal period for $\bar{B}_{||}$ [111]. The intercept and slope are used to calculated m_1 and E_g from equation (10).

and the higher conduction band states are important in determining the valance band parameters.

The interaction of the electron spins with the magnetic field splits each Landau level by an amount $\pm g e\hbar B/4\, m_o c$, where the electron g-factor depends on the electron spin-orbit interaction. The two series of quantum oscillations associated with the two spin orientations interfere, producing a single set of quantum oscillations with an amplitude controlled by the factor $\cos(\pi g \mu/2)$, where μ is the normalized cyclotron mass appropriate to the applied field direction. Knowledge of this factor is important in our amplitude analysis.

The g-factor is related to the components of a second-rank tensor and in PbTe has a directional dependence of the form (refs. 35 and 36)

$$g^2 = g_{||}^2 \cos^2\theta + g_{\perp}^2 \sin^2\theta \tag{11}$$

where $g_{||}$ and $g_{\perp}$ are the g-factors for the field parallel and perpendicular to the [111] axis. The results of a number of different experiments (table I) indicate that at the band

TABLE I. - SPIN SPLITTING FACTORS AND g-VALUES FOR p-TYPE LEAD TELLURIDE

Experiment source	Carrier concentration, cm^{-3}	Effective mass g-factor				Band-edge effective mass, μ_3	$g_{\parallel}$
		$(g\mu/2)_{\langle 100\rangle}$	$\mu_{\langle 100\rangle}$	$g_{\langle 100\rangle}$	$g_{\parallel}\mu_t/2$		
Ref. 34	[a]0	---	---	[b]29	---	---	---
Ref. 27	0	---	---	---	---	---	51±8
This report; sample X6	$.9\times10^{18}$	0.65±0.05	[c]0.041±0.004	32±4	---	0.027±0.002	[d]48±5
Ref. 37	3.0	.58±0.01	.051±0.008	23±5	0.58±0.01	.036±0.002	32±2
This report; sample X5	3.5	.55±0.05	[c].055±0.002	20±2	---	.038±0.001	[d]29±3
Ref. 32	4	---	---	---	[e].58±0.03	.040±0.008	29±6
Ref. 32	6	---	---	---	[e].53±0.02	.044±0.009	24±5

[a]p-n junction.
[b]Assuming conduction and valence band g-factors equal.
[c]Computed from eq. (A9).
[d]Assuming $g\mu$ to be the same along $\langle 111\rangle$ and $\langle 100\rangle$.
[e]Using a different splitting scheme than Schilz.

edge, $g_{\parallel} \cong 50$ and that $g_{\parallel}$ decreases with increasing carrier concentration. Burke, Houston, and Savage (ref. 37) find $g_{\perp} = 7\pm2$. The carrier concentration dependence of $g_{\parallel}$ is related to the nonparabolicity of the bands; the interband interactions which determine the g-factor are quite similar to those which determine the inverse effective mass. To a first approximation, both experimentally and theoretically (refs. 35 and 36) $g_{\parallel}$ varies with carrier concentration as $1/m_t$. Schilz (ref. 32) found the spin factor $g\mu/2$ to be directionally independent. This is borne out by other work; for example, using the values of Burke, Houston, and Savage (ref. 37) and equations (A9) and (11) we compute $g\mu/2$ to be 0.56 for the ellipsoid with the smallest extremal area when $\vec{B}$ is along [110]. This value is sensibly the same as the values 0.58 shown in table I for the [100] and [111] directions. Since we were able to measure the spin splitting only with $\vec{B}\parallel[100]$, we will assume the amplitude factor $\cos(\pi g\mu/2)$ to be the same for the [100], [110], and [111] directions.

The effect of strain on nondegenerate[1] energy levels in semiconductors can be described by a deformation potential tensor $\overleftrightarrow{\Xi}$ (refs. 38 to 40). In this scheme the shift in the energy of the point ν in a band is described to first order in the strain $\overleftrightarrow{\epsilon}$ by $\delta E^{\nu} = \overleftrightarrow{\Xi}^{\nu} : \overleftrightarrow{\epsilon}$. In general, each point in the band will have nine deformation potentials

[1]There is, in fact, the spin degeneracy; however, for the rock salt structure, this degeneracy is never destroyed by strain deformation (ref. 41).

associated with it. However, this number is usually greatly reduced at a symmetry point. At the L-points in PbTe there are only two independent deformation potentials for each band, and we can express $\overleftrightarrow{\Xi}^{\nu}$, using the notation of Herring (refs. 39 and 40), as $\Xi_{ij}^{\nu} = \Xi_d \delta_{ij} + \Xi_u u_i^{\nu} u_j^{\nu}$ where δ_{ij} is the Kronecker delta and the unit vector $\hat{u}$ points to a particular L-point. This leads to an energy shift of the form

$$\delta E^{\nu} = \left(\Xi_d + \frac{1}{3}\Xi_u\right)(\epsilon_1 + \epsilon_2 + \epsilon_3) + \frac{1}{3}\Xi_u(\pm\epsilon_4 \pm \epsilon_5 \pm \epsilon_6) \tag{12}$$

where the signs depend upon ν. The PbTe deformation potentials have been calculated by Ferreira (ref. 41). However, there has been only a limited amount of experimental work on determining the PbTe deformation potentials. Ferreira's results are shown in table II along with the deformation potentials derived from piezoresistance measurements

TABLE II. - DEFORMATION POTENTIALS OF LEAD TELLURIDE

Type of data	Source	Valence band		Conduction band	
		Deformation potential, eV			
		Ξ_d^v	Ξ_u^v	Ξ_d^c	Ξ_u^c
Theory	Ref. 42	-8.93	10.46	-4.36	8.29
Experiment	Ref. 43	-----	5.6	-----	3.8
		-----	8.5	-----	----

by Ilisavskii (ref. 42) and Burke (ref. 43). In order to find the deformation potential from piezoresistance, the elastic constants and the ratio of the mobilities perpendicular and parallel to the [111] axis must be known. Ilisavskii did not have good values for these two parameters, so we have recalculated his deformation potentials using Burke's latest values. The variation of the energy gap with pressure has been measured optically (ref. 44) giving $\left(3\Xi_d^c + \Xi_u^c\right) - \left(3\Xi_d^v + \Xi_u^v\right) = 9.5$ to 11.4 electron volts, where the superscripts refer to the valance or conduction bands. Ferreira's theoretical values give 11.6 electron volts, in reasonable agreement with experiment.

The band edge masses m_1 and m_3 are found in the work of Lin and Kleinman (ref. 25) to be approximately given by $m_0/m_i = M_i/\Delta$, where the $M_i (i = 1, 3)$ are appropriate momentum matrix elements. Since we expect these matrix elements to be insensitive to small strains, we find, using equation (12),

$$\frac{\partial \ln m_{1,3}}{\partial \epsilon_i} = \frac{\partial \ln \Delta}{\partial \epsilon_i}$$

$$= \begin{cases} \dfrac{G_1}{\Delta} & \text{for } i = 1, 2, \text{ or } 3 \\ \pm \dfrac{G_2}{\Delta} & \text{for } i = 4, 5, \text{ or } 6 \end{cases} \tag{13}$$

where

$$\left.\begin{aligned} G_1 &= \left(\Xi_d^c - \Xi_d^v\right) + \frac{1}{3}\left(\Xi_u^c - \Xi_u^v\right) \\ G_2 &= \frac{1}{3}\left(\Xi_u^c - \Xi_u^v\right) \end{aligned}\right\} . \tag{14}$$

and the sign depends on the particular L-point considered. Since the g-values depend on the energy gap in a similar manner, they should have a similar type of strain dependence.

THEORY OF OSCILLATING MECHANICAL EFFECTS

Thermodynamic Relations

We obtain theoretical expressions (e.g., ref. 45) for the magnetostriction and magnetoelastic oscillations by considering the free-energy density of the crystal in a magnetic field as the sum of the zero-field elastic energy and the free energy of the diamagnetic electronic system Ω:

$$F(\vec{\epsilon}, T, H) = \frac{1}{2} \sum_{i,j=1}^{6} c_{ij}^{o} \epsilon_i \epsilon_j + \Omega(\vec{\epsilon}, T, B) + 2\pi M^2 \tag{15}$$

where the c_{ij}^{o} are zero-field components of the elastic stiffness tensor. The magnetization can be obtained from this free energy as (ref. 45) $M = -\partial F/\partial H = -\partial \Omega/\partial B$ and the stress as $\sigma_i = \partial F/\partial \epsilon_i$. The explicit dependence of the chemical potential on the strain,

temperature, and magnetic field is neglected since far from the quantum limit (the approximation considered here) its contribution to the oscillatory free energy will be small. Since we are interested in oscillatory effects, we need consider only the oscillatory part of Ω. For this we use the Lifshitz-Kosevich expression in the modified form given by Williamson, Foner, and White (ref. 46):

$$\Omega = \sum_{\nu} \sum_{\lambda=1}^{\infty} A_{\lambda\nu} \cos\left[\left(\frac{\lambda c S_m^{\nu}}{e\hbar B}\right) - \varphi_{\lambda}\right] \tag{16}$$

where $A_{\lambda\nu}$ is a temperature-dependent amplitude function that varies slowly with field,

$$A_{\lambda\nu} = 2kT\left(\frac{eB}{hc}\right)^{3/2} \left|\frac{\partial^2 S^{\nu}}{\partial p_B^2}\right|_{S^{\nu}=S_m^{\nu}}^{-1/2} \frac{\exp\left(\frac{-\lambda\alpha\mu_{\nu}T_D}{B}\right)\cos\left(\frac{\lambda\pi g_{\nu}\mu_{\nu}}{2}\right)}{\lambda^{3/2}\sinh\left(\frac{\lambda\alpha\mu_{\nu}T}{B}\right)} \tag{17}$$

where μ_{ν}, g_{ν}, and S_m^{ν} are, respectively, the reduced cyclotron mass, the effective g-factor, and the extremal cross-sectional area of the ν^{th} sheet of the Fermi surface, T_D is the Dingle temperature representing the effect of electron scattering, and $\alpha = 2\pi^2 k m_o c/\hbar e$. The phase factor is $\varphi_{\lambda} = 2\pi\lambda\gamma \pm \pi/4$, where γ is the phase associated with the Landau quantization; the upper sign is used when S_m^{ν} is a maximum, the lower for a minimum. From equation (15) we find the general expression for the strain:

$$\epsilon_1 = \sum_{j=1}^{6} s_{ij}^{o}\left(\sigma_j - \frac{\partial\Omega}{\partial\epsilon_j} - 4\pi M\frac{\partial M}{\partial\epsilon_j}\right) \tag{18}$$

where the s_{ij}^{o} are defined by $\sum_{j=1}^{6} s_{ij}^{o} c_{jk}^{o} = \delta_{ik}$. In PbTe the magnetization is small enough so that the last term in equation (18) can be neglected. (Also, because of the smallness of M, the difference between B and H is inconsequential in our analysis.) The oscillatory magnetostriction in the $[l, m, n]$ direction for a PbTe crystal with zero (or constant) external stresses is thus described by the equation

$$\epsilon_{\ell mn} = -\sum_{i,j=1}^{6} \frac{\partial \epsilon_{\ell mn}}{\partial \epsilon_i} s^o_{ij} \frac{\partial \Omega}{\partial \epsilon_j} \tag{19}$$

where $\partial \epsilon_{\ell mn}/\partial \epsilon_i$ is a product of direction cosines,

$$\epsilon_{\ell mn} = \ell^2 \epsilon_1 + m^2 \epsilon_2 + n^2 \epsilon_3 + mn\epsilon_4 + \ell n \epsilon_5 + \ell m \epsilon_6$$

The inverse of Young's modulus in the $[\ell, m, n]$ direction is defined by $(Y_{\ell mn})^{-1} \equiv \partial \epsilon_{\ell mn}/\partial \sigma_{\ell mn}$; therefore the ME oscillations are given by

$$Y^{-1}_{\ell mn}(B) - Y^{-1}_{\ell mn}(0) \equiv \Delta(Y_{\ell mn})^{-1} = -\sum_{i,j,k,t=1}^{6} \frac{\partial \epsilon_{\ell mn}}{\partial \epsilon_i} s^o_{ij} \frac{\partial \sigma_k}{\partial \sigma_{\ell mn}} \times \frac{\partial \epsilon_t}{\partial \sigma_k} \frac{\partial^2 \Omega}{\partial \epsilon_j \partial \epsilon_t} \tag{20}$$

Using the identity $\partial \sigma_k/\partial \sigma_{\ell mn} = \partial \epsilon_{\ell mn}/\partial \epsilon_k$ and the approximation $\partial \epsilon_t/\partial \sigma_k \cong s^o_{tk}$, the ME oscillations are thus described to first order in the elastic constants by

$$\Delta(Y_{\ell mn})^{-1} = -\sum_{i,j,k,t=1}^{6} \frac{\partial \epsilon_{\ell mn}}{\partial \epsilon_i} \frac{\partial \epsilon_{\ell mn}}{\partial \epsilon_j} s^o_{ik} s^o_{jt} \frac{\partial^2 \Omega}{\partial \epsilon_k} \partial \epsilon_t \tag{21}$$

Strain Derivatives of the Free Energy

In order to evaluate the strain derivatives of the free energy Ω we need to evaluate the strain derivatives of the various band parameters which appear in Ω. To this end, we next use our model of the PbTe band structure to express the strain dependence of the effective masses and cross-sectional areas in terms of the strain dependence of the Fermi energy and the band gap. We then obtain expressions for the strain dependence of these two characteristic energies in terms of the deformation potential parameters.

The band shifts described by the deformation potential scheme lead to variations in Ω via three types of effects. The first is due to the relative shift of the valleys produced by a shear strain. Under a shear, some of the valleys move up in energy and some move down. This relative shift of the valleys is accompanied by intervalley charge transfer and changes in the Fermi surface cross-sectional areas. Second are effects due to the nonparabolic bands. Since the energy bands of PbTe are nonparabolic, a shift in the Fermi energy also produces a change in the band parameters. Third are the effects due to the strain dependence of the energy gap. The conduction and valance band deformation potentials are different; therefore, the energy gap is strain dependent. A change in the gap produces a change in the curvature of the bands, hence a change in band parameters. The first effect can occur only with a shear strain, whereas the last two effects will accompany both shear the dilatation strains. We will see from what follows that the dominant effect in PbTe is due to the intervalley charge transfer. This is evidenced experimentally by the fact that both the [100] ME and MS oscillations, which are the only ones to come from pure dilatation strains and involve no intervalley charge transfer, are at least an order of magnitude smaller than the oscillations along other axes.

We account quantitatively for the strain dependence of the cyclotron and band masses by differentiating equations (A9) and (A5):

$$\frac{\partial \ln \mu}{\partial \epsilon_i} = C_t(\mu) \frac{\partial \ln \mu_t}{\partial \epsilon_i} + \left[1 - C_t(\mu)\right] \frac{\partial \ln \mu_l}{\partial \epsilon_i} + C_\theta(\mu) \frac{\partial \theta}{\partial \epsilon_i} \tag{22}$$

$$\frac{\partial \ln m^*}{\partial \epsilon_i} = C_t(m^*) \frac{\partial \ln m_t}{\partial \epsilon_i} + \left[1 - C_t(m^*)\right] \frac{\partial \ln m_l}{\partial \epsilon_i} + C_\theta(m^*) \frac{\partial \theta}{\partial \epsilon_i} \tag{23}$$

where

$$C_t(\mu) = \left(\frac{\mu}{\mu_t}\right)^2 \left[\cos^2\theta + \frac{\mu_t}{2\mu_l} \sin^2\theta\right] \tag{24}$$

and

$$C_\theta(\mu) = \left(\frac{\mu}{\mu_t}\right)^2 \cos\theta \sin\theta \left(1 - \frac{\mu_t}{\mu_l}\right) \tag{25}$$

and $C_t(m^*)$ and $C_\theta(m^*)$ are obtained from equations (24) and (25) by replacing μ, μ_t, and μ_l with m^*, m_t, and m_l, respectively. From equations (7) and (A9) we see that the transverse masses are functions of both the Fermi energy and the energy gap. There is a further energy-gap dependence of the band edge masses, m_1 and m_3, which we discussed in a previous section. Assuming that the effective gap is proportional to the direct gap, $E_g \propto \Delta$, simple differentiation gives the relations

$$\frac{\partial \ln \mu_t}{\partial \epsilon_i} = C_F \frac{\partial \ln E_F}{\partial \epsilon_i} + C_g \frac{\partial \ln E_g}{\partial \epsilon_i} \tag{26}$$

and

$$\frac{\partial \ln \mu_l}{\partial \epsilon_i} = \frac{\partial \ln E_g}{\partial \epsilon_i} \tag{27}$$

where

$$C_F = \frac{2 \dfrac{E_F}{E_f}}{1 + 2 \dfrac{E_F}{E_g}} \tag{28}$$

and

$$C_g = \frac{1 + \dfrac{E_F}{E_g}}{1 + 2 \dfrac{E_F}{E_g}} \tag{29}$$

and, further,

$$\frac{\partial \ln m_t}{\partial \epsilon_i} = C_m \frac{\partial \ln E_F}{\partial \epsilon_i} + (1 - C_m) \frac{\partial \ln E_g}{\partial \epsilon_i} \tag{30}$$

and

$$\frac{\partial \ln m_l}{\partial \epsilon_i} = \frac{\partial \ln E_g}{\partial \epsilon_i} \tag{31}$$

where

$$C_m = \frac{\dfrac{E_F}{E_g}}{1 + \dfrac{E_F}{E_g}} \tag{32}$$

Equations (22) to (32) express the strain dependence of μ and m^* in terms of the strain dependence of the energy gap, the Fermi energy, and the angle between the spheroid axis and the magnetic field.

From equation (A6) we see that the strain dependence of the extremal cross-sectional area is

$$\frac{\partial \ln S_m}{\partial \epsilon_i} = \frac{\partial \ln m^*}{\partial \epsilon_i} + \frac{\partial \ln E_F}{\partial \epsilon_i} \tag{33}$$

Thus, using equation (23), (30) and (30) with equation (33), we are also able to express $\partial \ln S_m / \partial \epsilon_i$ in terms of the strain dependence of E_g, E_F, and θ.

We have assumed that $E_g \propto \Delta$; therefore $\partial \ln E_g / \partial \epsilon_i = \partial \ln \Delta / \partial \epsilon_i$, which is given by equation (13). The strain dependence of the Fermi energy is computed using the constraint that the total number $\mathscr{P}$ of carriers in the sample is independent of the strain. For our spheroidal model (see eq. (A1)), the density of carriers in the ν^{th} valley is

$$p_\nu = \frac{2^{3/2}}{3\pi^2 \hbar^3} m_t m_l^{1/2} \left(E_F^\nu\right)^{3/2} \tag{34}$$

Since $\mathscr{P} = V \sum_{\nu=1}^{4} p_\nu$, where V is the crystal volume, the constraint $\partial \mathscr{P} / \partial \epsilon_i = 0$ leads directly to

$$\delta_{1i} + \delta_{2i} + \delta_{3i} + \frac{1}{4}\left[\left(\frac{3}{2} - C_m\right)\sum_{\nu=1}^{4} \partial \ln \frac{E_g^\nu}{\partial \epsilon_i} + \left(\frac{3}{2} + C_m\right)\sum_{\nu=1}^{4} \partial \ln \frac{E_F^\nu}{\partial \epsilon_i}\right] = 0 \qquad (35)$$

where δ_{ij} is the Kronecker symbol, and we have used equations (30) to (32) to express the strain derivatives of m_t and m_l in terms of the strain derivatives of E_g^ν and E_F^ν. The Fermi energy for our p-type samples is the difference between the chemical potential ζ and the valance band maximum E_V^ν; therefore,

$$\frac{\partial \ln E_F^\nu}{\partial \epsilon_i} = \frac{1}{E_F}\left(\frac{\partial E_V^\nu}{\partial \epsilon_i} - \frac{\partial \zeta}{\partial \epsilon_i}\right) \qquad (36)$$

Using the valence band shifts and the gap dependence described by the deformation potential scheme, equations (12), (13), (35), and (36) lead to expressions for $\partial \ln E_F^\nu / \partial \epsilon_i$ in terms of the deformation potentials. There are two cases to be considered:

(1) dilatational strain (i = 1, 2, or 3). Equations (12) and (13) indicate that all the gap and band-edge shifts are independent of ν. Therefore, the sums in equation (35) are replaced by a multiplication factor of four, giving

$$\frac{\partial \ln E_F^\nu}{\partial \epsilon_i} = -\frac{\frac{2}{3} + \left(1 - \frac{2}{3} C_m\right)\frac{G_1}{\Delta}}{1 + \frac{2}{3} C_m} \qquad (37)$$

(2) shear strain (i = 4, 5, or 6). From equations (12) and (13)

$$\sum_{\nu=1}^{4} \frac{\partial \ln E_V^\nu}{\partial \epsilon_i} = 0$$

and

$$\sum_{\nu=1}^{4} \frac{\partial \ln E_g^\nu}{\partial \epsilon_i} = 0$$

From these and equations (35) and (36), it follows that $\partial\xi/\partial\epsilon_i = 0$, so that

$$\frac{\partial \ln E_F^\nu}{\partial \epsilon_i} = \frac{1}{E_F^\nu}\frac{\partial E_V^\nu}{\partial \epsilon_i} = \pm\frac{1}{3}\frac{\Xi_u}{E_F^\nu} \tag{38}$$

We next examine the strain derivatives of Ω which appear in the expression for the MS and ME oscillations, equations (19) and (21), using the expressions for the strain derivatives of the band parameters (eqs. (22) to (38)). Equations (16) and (17) indicate that $\partial\Omega/\partial\epsilon_i$ contains many strain derivatives since the effective masses, g-factor, Dingle temperature, cross-sectional area, and volume are, in principle, all strain dependent. However, by completely differentiating equations (16) and (17) and numerically evaluating the various terms using the parameters appropriate to our PbTe samples, we find that the contribution from the strain derivative of S_m^ν in the argument of the cosine factor is at least an order of magnitude larger than any other contribution. (In this numerical analysis, we assume that $\partial \ln T_D/\partial\epsilon_i$ and $\partial \ln g/\partial\epsilon_i$ are at most as large as $\partial \ln \mu/\partial\epsilon_i$. Also, since the crystal strains never exceeded 10^{-6} in our experiments and the cubic symmetry was only slightly perturbed, we can assume that $\partial\theta/\partial\epsilon_1 \lesssim 1$. This is equivalent to assuming that the Fermi surface ellipsoids continue to point very nearly along the body diagonals of the strained cubic lattice.) Schematically,

$$\frac{\partial\Omega}{\partial\epsilon_i} = \frac{\partial A}{\partial\epsilon_i}\cos\left[\frac{cS_m}{e\hbar B} - \varphi\right] - A\,\frac{cS_m}{e\hbar B}\,\frac{\partial \ln S_m}{\partial\epsilon_i}\sin\left[\frac{cS_m}{e\hbar B} - \varphi\right]$$

Since we find that $\partial \ln A/\partial\epsilon_i$ is roughly of the same order as (or less than) $\partial \ln S_m/\partial\epsilon_i$, one of the principal factors that determine the relative magnitude of the various terms is $cS_m/(e\hbar B)$. This number is equal to 2π times the number of Landau levels below the Fermi surface. Since our amplitude measurements were always made with oscillations corresponding to Landau numbers greater than five, the $\partial \ln S_m/\partial\epsilon_i$ term dominates. The fact that this is the dominant term is also borne out experimentally by the observed phase of the MS oscillations. The amplitude analysis in this work is made with that part of the data which show only a single period. These periods correspond to the smallest extremal area which we label S_m^o. Since numerical evaluation shows that the contributions to $\partial\Omega/\partial\epsilon_i$ from other extremal areas and from harmonics ($\lambda > 1$) are negligible, the expression that we use for our MS amplitude analysis takes the form

$$\frac{\partial \Omega}{\partial \epsilon_i} \sim -A_{10} \frac{cS_m^o}{e\hbar B} \sum_{S_m^o} \frac{\partial \ln S_m^o}{\partial \epsilon_i} \sin\left(\frac{cS_m^o}{e\hbar B} - \varphi_1\right) \tag{39}$$

where the sum is over all the equivalent pieces of the Fermi surface which contribute to the given period.

We further find from numerical evaluation of the various terms in the second strain derivatives of Ω that under the experimental conditions just discussed we can write

$$\frac{\partial^2 \Omega}{\partial \epsilon_i \, \partial \epsilon_j} \simeq -A_{10} \left(\frac{cS_m^o}{e\hbar B}\right)^2 \sum_{S_m^o} \frac{\partial \ln S_m^o}{\partial \epsilon_i} \frac{\partial \ln S_m^o}{\partial \epsilon_j} \cos\left(\frac{cS_m^o}{e\hbar B} - \varphi_1\right) \tag{40}$$

Equation (40) could include terms in $\partial^2 S_m^o / \partial \epsilon_i \, \partial \epsilon_j$; however, a comparison of phases of the MS and ME oscillations shows that such terms are negligible.

Analytic Expressions and Ratio

Equations (19) and (39) and equations (21) and (40) combine to give the expressions that we use in analyzing our MS and ME experimental data,

$$\epsilon_{l\,mn} = A_{10} \frac{cS_m^o}{e\hbar B} \sum_{S_m^o} \sum_{i,j=1}^{6} \frac{\partial \epsilon_{l\,mn}}{\partial \epsilon_i} s_{ij}^o \frac{\partial \ln S_m^o}{\partial \epsilon_j} \sin\left(\frac{cS_m^o}{e\hbar B} - \varphi_1\right) \tag{41}$$

$$\Delta(Y_{l\,mn})^{-1} = A_{10} \left(\frac{cS_m^o}{e\hbar B}\right)^2 \sum_{S_m^o} \left(\sum_{i,j=1}^{6} \frac{\partial \epsilon_{l\,mn}}{\partial \epsilon_i} s_{ij}^o \frac{\partial \ln S_m^o}{\partial \epsilon_i}\right)^2 \cos\left(\frac{cS_m^o}{e\hbar B} - \varphi_1\right) \tag{42}$$

In our analysis of the experimental data, we fit the MS data to equation (41) and separately fit the ME data to equation (42). We determine experimentally the values of A_{10} and S_m^o and find experimental values for the strain derivative sums which we then relate to the deformation potentials. From equations (41) and (42) we see that the complicated coefficient A_{10} should disappear from the expression for the ratio of the MS and ME amplitudes for a given sample under the same thermodynamic conditions, that is, the same B, T, crystallographic orientation, etc. However, we find the MS and ME Dingle temperatures T_D^ϵ and T_D^Y to be different, leading to a term $\exp\left[\alpha\mu\left(T_D^\epsilon - T_D^Y\right)/B\right]$ in the expression for the ratio. Even then, consideration of the ratio leads to a considerable simplification of the analysis, and we use the ratio in a separate approach to analyze the deformation potential.

EXPERIMENTAL METHODS

The oscillatory magnetostriction was measured by determining the change in capacitance of a parallel-plate capacitor composed of one fixed plate and one plate glued directly to the end of the oriented single crystal PbTe sample. We used a three-terminal capacitance cell based on a differential thermal expansion cell described by White (ref. 47), modified to allow a variety of samples with different dimensions to be used in one cell. A ratio transformer bridge (General Radio 1615-A) and a phase-sensitive null detector were used to measure the change in capacitance. This technique allowed us to detect a change in capacitance of the order of 10^{-6} picofarad, which corresponded to strains of a few times 10^{-10}.

The magnetoelastic oscillations were measured using the mechanical composite oscillator technique developed by Quimby and Balamuth (refs. 48 and 49). The composite oscillator consisted of a quartz bar (typical dimensions 1 by 0.25 by 0.25 cm) bonded to an oriented single crystal PbTe bar of identical transverse dimensions. The long axis of the quartz transducer was in the Y quartz direction. The X-faces of the quartz were coated with chromium-gold electrode films so that a Young's modulus vibrational mode for the composite system was excited when a sinusoidal voltage was applied to the electrodes. The electrical leads, which also served to support the oscillator, were attached to the transducer at nodal points. The composite oscillator was driven by a frequency-stable constant-voltage source, usually at a frequency near the fundamental resonance of the transducer (typically 250 kHz). Changes in the Young's modulus of the sample as a result of an applied magnetic field produced changes in the resonance frequency of the composite oscillator (appropriate analytic expressions are given by Balamuth (ref. 49)),

which, in turn, produced changes in the electrical impedance of the oscillator circuit. This impedance change was detected directly by monitoring the voltage across a small series resistor. The voltage was amplified, rectified, and applied to an X-Y recorder. The response of the composite oscillator was investigated as a function of magnetic field at several driving frequencies on each side of the resonance as well as at the resonance peak itself in order to compare the changes in dispersion and attenuation of the system. In the 250-kilohertz range, attenuation effects were completely negligible compared with the resonance frequency shifts due to changes in the PbTe Young's modulus. Because of the high Q of the composite oscillator (typically 10^3 to 10^4), the sensitivity was high; the minimum detectable fractional change in Young's modulus was estimated to be 10^{-6} to 10^{-7}. It is noteworthy that even in its relatively unsophisticated form this system compares favorably in sensitivity with the "sing-around" ultrasonic technique commonly used to measure sound velocity changes (ref. 44).

Details of the MS and ME experimental techniques and apparatus have been described elsewhere by one of us (T.E.T.) (ref. 50).

EXPERIMENTAL RESULTS AND DISCUSSION

Band Parameters

Our experiments were performed on single-crystal samples from two different boules of p-type material grown by one of us (T.E.T.) by the Czochralski method. The boules were labeled X5 and X6. Samples were spark cut from neighboring sections of the middle of the boules. Hall measurements gave carrier concentrations of $(3.5\pm0.2)\times10^{18}$ per cubic centimeter for the X5 samples and $(0.9\pm0.1)\times10^{18}$ per cubic centimeter for the X6 samples. The X5[110] sample was a 0.851- by 0.488- by 0.462-centimeter bar with the long axis parallel to [110]. The X5[100]-stack was 0.927- by 0.353- by 0.36-centimeter [100]-oriented bar produced by gluing two nearly cubical pieces together with GE7031 varnish. The stacking was done to increase the OM signal. No magnetoelastic oscillation experiments were made with the samples from X5. The three X6 bars with axes along [100], [110], and [111] had dimensions 0.749 by 0.274 by 0.312 centimeter, 0.745 by 0.282 by 0.244 centimeter, and 0.805 by 0.269 by 0.257 centimeter, respectively.

The oscillation periods and phases were analyzed in terms of the factors $\cos[2\pi/(PB) - \varphi_1]$ in equations (41) and (42). The period and phase were found by assigning successive integers N to the oscillation peaks and plotting the inverse magnetic field for the N^{th} peak, B_N^{-1}, against N. The major oscillation periods found in this manner from the complete set of experiments are presented in table III. The errors quoted are

TABLE III. - MEASURED OSCILLATION PERIODS AND CYCLOTRON MASSES

Field direction	Oscillation period, T^{-1}		Cyclotron mass, m_o	
	Sample			
	X5	X6	X5	X6
$\vec{B}\parallel[100]$	----------	$(10.9\pm0.2)\times10^{-2}$	----------	----------
$\vec{B}\parallel[110]$	$(5.46\pm0.03)\times10^{-2}$	(14.6 ± 0.2)	0.047 ± 0.003	0.033 ± 0.003
$\vec{B}\parallel[111]$	(6.55 ± 0.07)	(18.0 ± 0.3)	$.038\pm0.001$	$.027\pm0.002$

a combination of the standard deviation of the mean found from a least-squares fit of the data and the 0.5 percent field calibration uncertainty of the magnets. These periods are in agreement with those found in reference 27.

An important consideration in the analysis was the relative phases of the MS and ME oscillations. As equations (40) and (41) show, the ME and MS oscillations for a particular sample and field orientation should be 90° out of phase if our model is correct. We observe this phase relation in our data (fig. 3). The sign of the oscillations depends on the sign of $\sum_{i,j=1}^{6} (\partial \epsilon_{l\,mn}/\partial \epsilon_i) s^o_{ij} (\partial \ln S^o_m/\partial \epsilon_j)$ and the sign of A_{10}. We find that all our data fit consistently into our analytical picture if we assume that $\gamma = 1/2$. This value of γ leads to a negative value for A_{10}, which from equation (17) corresponds to a negative value for $\cos(\pi g \mu/2)$. This sign for $\cos(\pi g \mu/2)$ is in agreement with the $g\mu$ values presented in table I. A least-squares fit of all the phases within this scheme gives $\gamma = 0.49\pm0.01$.

For the spheroidal model described by equations (3), (5), and (6) the carrier density p needed to fill four spheroids is related to the oscillation period P and the mass anisotropy $K \equiv m_l/m_t$ by

$$p = aP^{-3/2}(K\cos^2\theta + \sin^2\theta)^{3/4}K^{-1/4} \tag{43}$$

where θ is the angle between the major axis of the spheroid, that is, [111], and the applied magnetic field and $a = 2.263\times10^{16}\ T^{-3/2}\ cm^{-3}$ (a product of universal constants). Using equation (43), the periods presented in table III, and the measured carrier concentrations, we find $K = 6.5(+1.0, -0.6)$ for X5 and $K = 8.3\pm0.9$ for X6. In figure 4 we have plotted our values for K along with values found in p-type PbTe by other workers. The two most recent studies, those by Burke, Houston, and Savage (ref. 37) and by Schilz (ref. 32) indicate K values that are twice as large as those found in our work and that of three other investigators (refs. 26 and 51 to 53). Burke (ref. 37) made an extensive

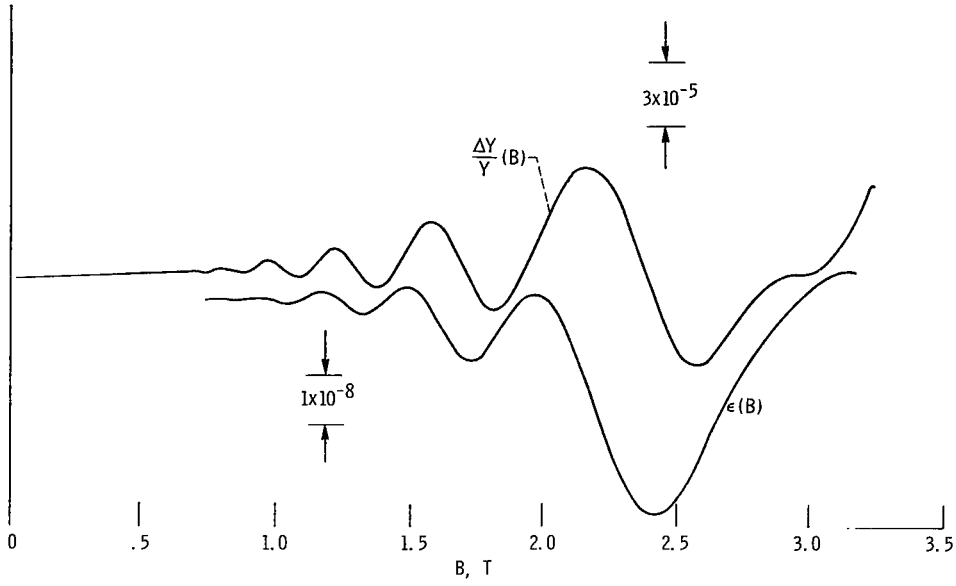

Figure 3. - Typical magnetostriction and magnetoelastic oscillation data. Sample X6[110]; field direction, $\vec{B} \parallel [111]$; Young's modulus and strain measured parallel to [110] direction; absolute temperature, 4.2 K.

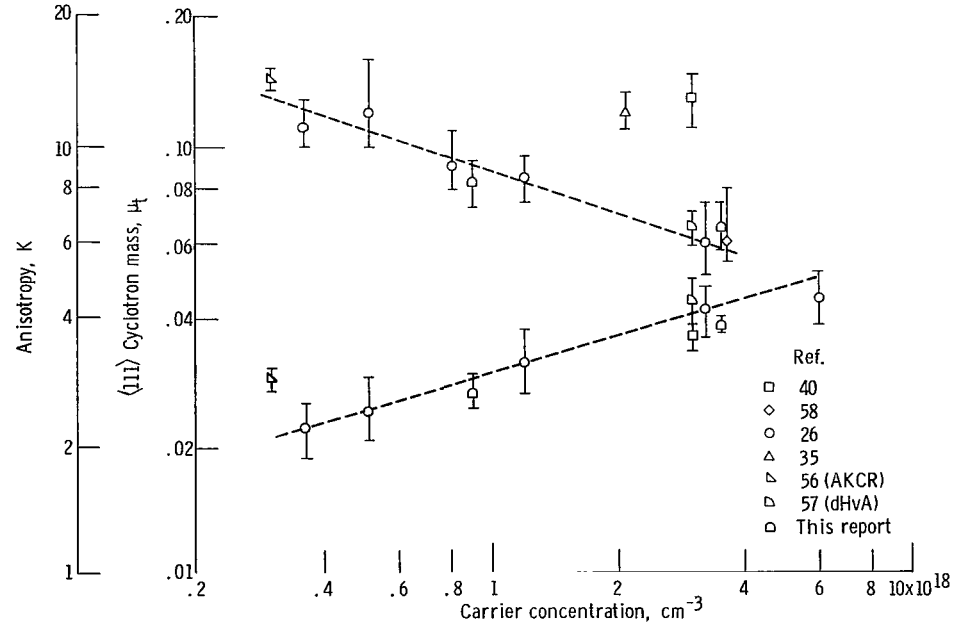

Figure 4. - Published values of the ⟨111⟩ cyclotron mass and the mass anisotropy K as function of carrier concentration for p-type lead telluride.

study of Shubnikov-de Haas frequencies. He Fourier-analyzed the frequency spectrum from the three fundamental oscillations and as many as five harmonics for numerous magnetic field directions in the (110) plane. It is quite difficult to understand the discrepancy between their results and the results of the other workers. It is noteworthy that Burke (ref. 37) finds that the carrier concentration determined from a high-field Hall measurement agrees with that determined from the best fit of their data to equation (43). In both the work of Stiles (ref. 52) and Cuff (ref. 26), the carrier concentration found from equation (43) was about 30 percent less than that determined from a Hall measurement for $p \simeq 3\times10^{18}$ per cubic centimeters. The latter authors attribute these extra carriers to other pieces of the Fermi surface. Analysis of Coste's data (ref. 53) gives reasonable agreement between the p from equation (43) and that from a Hall measurement.[2] Since the value of K comes into the amplitude analysis through the term $\left|\partial^2 S^\nu/\partial p_B^2\right|^{-1/2}$, (eqs. (17) and (A4)), the contradictory K values shown in figure 4 will be discussed further in the section Amplitudes. Unless otherwise stated we will use our experimental values for K.

Cyclotron effective masses were found by measuring the ratio of the MS oscillation amplitudes at two temperatures. From equations (41) and (17) the ratio of the amplitudes at the same magnetic field but at two different temperatures is given by

$$\frac{\epsilon(T_1, B)}{\epsilon(T_2, B)} = \frac{T_1 \sinh\left(\frac{\alpha\mu T_2}{B}\right)}{T_2 \sinh\left(\frac{\alpha\mu T_1}{B}\right)} \quad (44)$$

This equation was solved by Newton's method on a digital computer for a series of oscillation peaks and temperatures. Data were normally taken near 4.2, 6,5, and 8.5 K. From a weighted least-squares fitting of the data result the masses presented in table III. Since the MS amplitudes for $\vec{B}\|[100]$ were very small, no masses could be determined for this field direction. No temperature-dependence studies were made for the magnetoelastic oscillations.

From equations (3) and (9), $m_t = 1/2(m_1 + \mu_3 m_o)$ and $m_l = Km_t$. Thus, from the values just presented, $m_t/m_o = 0.028\pm0.002$ and 0.023 ± 0.002, and $m_l/m_o = 0.18\pm0.02$ and 0.19 ± 0.02 for the X5 and X6 samples, respectively.

---

[2]In his paper Coste claims that these two values do not agree, but his computation of p seems to be in error.

As a test of the internal consistency of the model, we computed the [110] cyclotron mass using equation (A9), m_t, the measured [111] cyclotron mass, and the measured K. The computed values are 0.044±0.002 and 0.032±0.002 for X5 and X6, respectively. The agreement between these values and the measured values shown in table III supports the self-consistency of the model and measurements.

The Fermi energy is easily computed from the de Haas-van Alphen period and the effective mass (see the appendix):

$$E_F = \frac{e\hbar}{m_o c}\left(\frac{Pm^*}{m_o}\right)^{-1} \tag{45}$$

From our data for $\vec{B}\|[111]$, where $m^* = m_t$, we find $E_F = 63\pm5$ and 28 ± 2 meV for samples X5 and X6, respectively.

Above 2 tesla (20 kG) the ME and MS oscillations begin to show a splitting of the oscillation peaks due to the Zeeman splitting of the Landau levels. From the oscillations for $\vec{B}\|[100]$, where all four ellipsoids have the same fundamental frequency, we were able to determine the spin splitting of the peaks. Each peak corresponds to a solution of the equation

$$\frac{1}{PB} = N \pm \frac{g\mu}{4} + \gamma + \frac{1}{8} \tag{46}$$

where the second term on the right accounts for the two spin levels for each Landau quantum number N. This term was found by indexing the oscillation peaks with a spin index and a quantum number and plotting N against $(B_N^{-1})_+$ and $(B_N^{-1})_-$. The resulting g-factors are compared in table I with those found in p-type material by other workers. Butler and Calawa (ref. 34) obtain their results from magnetoemission sutdies in diode lasers, Schilz (ref. 32) from magnetoacoustic attenuation oscillations, and Cuff (ref. 27) and Burke (ref. 37) from Shubnikov-de Haas oscillations. For both $\vec{B}\|[111]$ and $\vec{B}\|[110]$, there are additional oscillations from a second set of ellipsoids. This makes the analysis difficult, and it has not been carried through.

The value of $g\mu$ depends on the assignment of spin and quantum numbers to a set of oscillations. From the phase analysis mentioned previously, we know that $\cos(\pi g\mu/2)$ must be negative, but this condition does not determine a unique labeling of the oscillation peaks. The values for $g\mu/2$ in table I correspond to a spin splitting greater than half the Landau splitting. This scheme gives g values that agree with the values found by

Patel and Slusher (ref. 54) from spin-flip Raman scattering in n-type material[3] with $n = 10^{17}$ per cubic centimeter.

Amplitudes

The MS amplitude coefficients were found by fitting the strain oscillation amplitudes to equations (17) and (41). From the data we computed the quantities $y = \ln\left[\epsilon_{\ell mn} B^{-1/2} \times \sinh(\alpha\mu T/B)\right]$ for each oscillation peak and a linear least-squares fit was made to a plot of y against B^{-1}. From the equations, it follows that the slope of this plot gives the Dingle temperature and that the y intercept leads to a value for

$$\cos\left(\frac{\pi g \mu}{2}\right) \sum_{S_m^o} \sum_{i,j=1}^{6} \frac{\partial \epsilon_{\ell mn}}{\partial \epsilon_i} s_{ij}^o \frac{\partial \ln S_m^o}{\partial \epsilon_j}$$

This procedure necessitates a knowledge of S_m^o, μ, and $\left|\partial^2 S/\partial p_B^2\right|_{S=S_m^o}^{-1/2}$ for which we use the band parameters presented in the section Band Parameters and equation (A3). The Dingle temperatures found from the MS oscillations are presented in table IV. The

TABLE IV. - DINGLE TEMPERATURES FROM MAGNETOSTRICTION OSCILLATIONS

Sample	Strain direction	Field direction			
		$\vec{B} \parallel [110]$	$\vec{B} \parallel [1\bar{1}0]$	$\vec{B} \parallel [111]$	$\vec{B} \parallel [\bar{1}11]$
		Dingle temperature, K			
X5	[110]	5.4±0.5	5.2±0.5	-------	4.5±0.3
X6	[110]	9.2±0.4	8.3±0.5	-------	7.2±0.3
	[111]	-------	7.3±0.5	8.3±0.6	-------

[3]Because of the similarities between the PbTe conduction and valance bands, the g-values (as well as effective masses) should be comparable in n- and p-type material.

errors indicated are the standard deviation of the mean computed from the random error associated with the amplitude measurements and the uncertainty in μ. The magnetostriction amplitudes for X5[100] and X6[100] were too small to give reliable Dingle temperatures.

In table V the strain derivative sums determined from the experimental MS amplitudes are presented and compared with values computed from the theory presented in the section Strain Derivatives of the Free Energy. The theoretical values were computed using the deformation potentials from Ferreira's (ref. 41) theoretical work (table II), and the elastic constants measured by Houston, Strakna, and Belson.[4] The extrapolated T = 0 K values for the stiffness constants were used to compute the following compliance constants: $s_{11}^o + 2s_{12}^o = (0.731 \pm 0.007) \times 10^{-11}$ m^2N^{-1} and $s_{44}^o = (6.61 \pm 0.04) \times 10^{-11}$ m^2N^{-1}. The large uncertainties of the theoretical values result entirely from the uncertainty in $\cos(\pi g\mu/2)$. Even though $g\mu$ is experimentally determined to better than 10 percent, $\cos(\pi g\mu/2)$ has a large percentage uncertainty when the function nears zero. The values in table I lead to $\cos(\pi g\mu/2) = -(0.19 \pm 0.10)$ for X5 and $-(0.40 \pm 0.08)$ for X6. The errors in the experimental strain derivative sums are the standard deviation of the mean due to the uncertainty of the amplitude measurements and the uncertainties in μ and K. Because of the discrepancy between the K values found by different experimenters for $p \approx 3 \times 10^{18}$ per cubic centimeter there is an added degree of uncertainty about the experimental values for X5, since the amplitude analysis includes the term $\left|\partial^2 S^\nu / \partial p_B^2\right|^{-1/2}$, which is K dependent. For instance, if we were to use K = 13, the value of Burke, Houston, and Savage (ref. 40), rather than our experimental value (K = 6.5) all of the X5 experimental values in table V would be reduced by 23 percent for $\vec{B} \| [100]$, by 27 percent for $\vec{B} \| [110]$, and by 29 percent for $\vec{B} \| [111]$. Using K = 13 instead of 8.3 for X6 gives 17-, 19-, and 20-percent reductions, respectively, for these three cases. Since both $\cos(\pi g\mu/2)$ and $\left|\partial^2 S^\nu / \partial p_B^2\right|^{-1/2}$ cancel out of the expressions for the ratio of the ME and MS amplitudes, the large uncertainties of these parameters do not enter into the results of the ratio analysis.

Magnetostriction oscillations were investigated at temperatures from 4 to 9 K. No temperature dependence of the strain derivative sum was observed and the data in table V are the average of values over this temperature range. The oscillations in several cases were just barely detectable or were not seen at all. For these cases an upper limit for the amplitude coefficient is presented. We had no X5[111] sample. Because the amplitudes for X6[100] were quite small for transverse magnetic field configurations,

---

[4]Straight forward, although tedius, symmetry considerations appropriate to the m3m symmetry of PbTe can also be used to find these relations.

TABLE V. - EXPERIMENTAL AND THEORETICAL VALUES OF STRAIN DERIVATIVE SUMS[a] FROM MAGNETOSTRICTION OSCILLATIONS FOR SAMPLE X6 ($p = 9\times10^{17}$ cm^{-3}) AND SAMPLE X5 ($p = 3.5\times10^{18}$ cm^{-3})

[Theoretical values were computed using $\Xi_u^V = 10.46$ eV.]

Sample	Type of data	Strain direction								
		[b][100]			[110]				[111]	
		Field direction								
		[100]	[010]	[011]	[110]	$[\bar{1}10]$	[001]	$[\bar{1}\bar{1}1]$	[111]	$[\bar{1}10]$
		Strain derivative sum[a], m^2N^{-1}								
X5	Experimental	$<0.97\times10^{-10}$	$<0.42\times10^{-10}$	$<0.34\times10^{-10}$	$(6.5\pm0.5)\times10^{-10}$	$(6.3\pm0.7)\times10^{-10}$	$<0.85\times10^{-10}$	$(3.5\pm0.4)\times10^{-10}$	(c)	(c)
	Simple theory	$(0.04\pm0.02)\times10^{-10}$	$(0.04\pm0.02)\times10^{-10}$	$(0.02\pm0.01)\times10^{-10}$	$(6.9\pm3.6)\times10^{-10}$	$(7.0\pm3.7)\times10^{-10}$	$(0.04\pm0.02)\times10^{-10}$	$(3.5\pm1.8)\times10^{-10}$	$(6.9\pm3.6)\times10^{-10}$	$(4.6\pm2.4)\times10^{-10}$
	Full theory	(.19±0.10)	(.19±0.10)	(.13±0.07)	(9.2±4.9)	(9.5±5.0)	(.19±0.10)	(4.8±2.5)	(9.4±4.9)	(6.4±3.4)
X6	Experimental	$<4.7\times10^{-10}$	----------	----------	$(50\pm4)\times10^{-10}$	$(56\pm9)\times10^{-10}$	$<5.7\times10^{-10}$	$(22\pm1)\times10^{-10}$	$(38\pm3)\times10^{-10}$	$(22\pm3)\times10^{-10}$
	Simple theory	$(0.08\pm0.02)\times10^{-10}$	$(0.08\pm0.02)\times10^{-10}$	$(0.04\pm0.01)\times10^{-10}$	(32.9±6.6)	(32.9±6.6)	$(0.08\pm0.02)\times10^{-10}$	(16.5±3.3)	(32.9±6.6)	(22.0±4.4)
	Full theory	(.30±0.06)	(.30±0.06)	(.18±0.04)	(38.9±7.9)	(39.3±7.9)	(.30±0.06)	(19.8±4.0)	(39.2±7.8)	(26.2±5.2)

[a]Strain derivative sum $= \left| \cos(\pi g\mu/2) \sum_{S_m^o} \left[\sum_{i,j=1}^{6} (\partial\epsilon_{l\,mn}/\partial\epsilon_i) s_{ij}^o (\partial \ln S_m^o / \partial\epsilon_j) \right] \right|$

[b]Sample X5 was stacked to increase the MS signal.

[c]No sample.

we did not attempt to aline the field along specific crystallographic directions for transverse fields. These facts explain the absence of entries for the corresponding crystal and field orientations in table V.

Two sets of theoretical values are presented in table V. The "simple theory" values correspond to a rigid parabolic band model with infinite energy gap. In this model the strain mass term, $\partial \ln m^*/\partial \epsilon_i$ in equation (33), is neglected and $\partial \ln S_m^o/\partial \epsilon_i$ is considered to be due solely to the change in crystal volume (= -2/3) for dilatation strains (i = 1, 2, or 3) or due to intervalley charge transfer $\left(= 1/3\ \Xi_u^V/E_F^\nu\right)$ for shear strains (i = 4, 5, or 6). The values labeled "full theory" are computed using the model represented by equations (33), (22), (30), (31), (37), (38), and (13). As an example of the magnitudes of some of the numbers which enter the theoretical computations, $\partial \ln m^*/\partial \epsilon_i$, $\partial \ln E_F/\partial \epsilon_i$, and $\partial \ln S_m^o/\partial \epsilon_i$ for X6 with $\vec{B} \| [110]$ are presented in table VI.

TABLE VI. - REPRESENTATIVE THEORETICAL STRAIN DERIVATIVES FOR X6 WITH $\vec{B} \| [100]$

Type of theory	Value of i	Strain derivatives		
		$\frac{\partial \ln m^*}{\partial \epsilon_i}$	$\frac{\partial \ln E_F}{\partial \epsilon_i}$	$\frac{\partial \ln S_m^o}{\partial \epsilon_i}$
Simple	1, 2, or 3	0	-2/3	-2/3
	4, 5, or 6	0	124.5	124.5
Full	1, 2, or 3	12.6	-15.7	-3.1
	4, 5, or 6	23.5	124.5	148.0

The agreement between the experimental and theoretical values in table V is quite reasonable; however, due to the large uncertainty in the theoretical values, especially for the X5 data, a definitive quantitative analysis of the experimental and theoretical amplitude factors is not possible with the numbers presented in table V. The relative magnitudes and ratios of the various terms do confirm many of the aspects of the model we have presented. We can see this by writing the strain derivatives in a more transparent form. When evaluating the strain derivative sums for the strain and field directions shown in table V by means of the prescriptions described in the section Strain Derivatives of the Free Energy, one finds that, except for the case $\epsilon \| [110]$ with $\vec{B} \| [001]$, all the sums can be simplified into the sum of a dilatation term and a shear term of the form (ref. 55)

$$\sum_{S_m^o} \sum_{i,j=1}^{6} \frac{\partial \epsilon_{lmn}}{\partial \epsilon_i} s_{ij}^o \frac{\partial \ln S_m^o}{\partial \epsilon_j} = N_e(\beta_d + D\beta_s) \tag{47}$$

where N_e is the number of equivalent extremal areas S_m^o, $\beta_d = \left(s_{11}^o + 2s_{12}^o\right) \partial \ln S_m^o / \partial \epsilon_1$, $\beta_s = s_{44}^o \partial \ln S_m^o / \partial \epsilon_4$, and D is a direction cosine factor which takes the values 0, 1/2, -1/2, 1, and -1/3 for the directions $\langle 100 \rangle$, [110], [$1\bar{1}0$], [111], and [$11\bar{1}$], respectively, when the derivative indicated in β_s is performed on the extremal area of the [111]-spheroid. For the case $\epsilon \| [110]$ with $\vec{B} \| [001]$, the right side of equation (47) becomes simply $4\beta_d$. A significant aspect of the model is that in this case the shear terms cancel when summed over the four spheroids: the shear strain causes two of the valance band maxima to move up in energy, thereby increasing the extremal areas at the Fermi energy, and the other two move down, decreasing their areas. Comparing equation (47) with the experimental data in table V shows that, qualitatively, the data fit our theoretical model quite well. We find, for example, that $|\beta_s| >> |\beta_d|$; the full theory values in table VI lead to $\beta_d = -2.2 \times 10^{-11}$ square meters per newton and $\beta_s = 977 \times 10^{-11}$ square meters per newton. These values are typical of the large difference between the dilatation and shear contributions to the strain derivative sums predicted by our theoretical model, including other field directions and for sample X5. Since the shear term β_s is theoretically so much larger than the dilatation term β_d, any term in equation (47) that contains β_s will be much larger than terms which do not contain β_s.

From table V we see that for all cases where equation (47) shows contributions from only the dilatation strains (i.e., $\epsilon \| [100]$, D = 0, or $\epsilon \| [110]$ with $\vec{B} \| [001]$, the experimental values are at least an order of magnitude smaller than those for which equation (47) shows shear contributions. This result confirms one aspect of the model.

Another confirming aspect of the MS data comes from the ratios of various amplitude terms. Using equation (47) and assuming that $\beta_s >> \beta_d$, the strain derivative sums for $\vec{B} \| [110]$ with ϵ along [110], [$1\bar{1}0$], and [$11\bar{1}$] should be in the ratio 1/2:-1/2:-1/3. For $\vec{B} \| [111]$ with ϵ along [$11\bar{1}$] and [110] the ratio should be 1:-1/2. The data, as presented in table V and interpreted in light of the symmetries involved, are seen to be in good agreement with these predictions. Perhaps the most striking experimental confirmation of the model comes from the signs of the observed phases. As we pointed out the phases are in complete agreement with our model; for example, the MS oscillations for $\vec{B} \| [110]$ with $\epsilon \| [1\bar{1}0]$ and [$1\bar{1}0$] are 180^o out of phase, as we would expect from equation (47).

The observed changes in amplitude and the phase shifts of the MS oscillations due to cancellation of the shear terms as the magnetic field is rotated into the [001] direction in the (110) plane are shown by the experimental data in figure 5. The experimental results with $\vec{B}$ or ϵ along $\langle 100 \rangle$ are difficult to analyze because the strain amplitudes are quite small and any slight misalinement of the sample would produce an anomalously large signal. This fact is made quite apparent by figure 5.

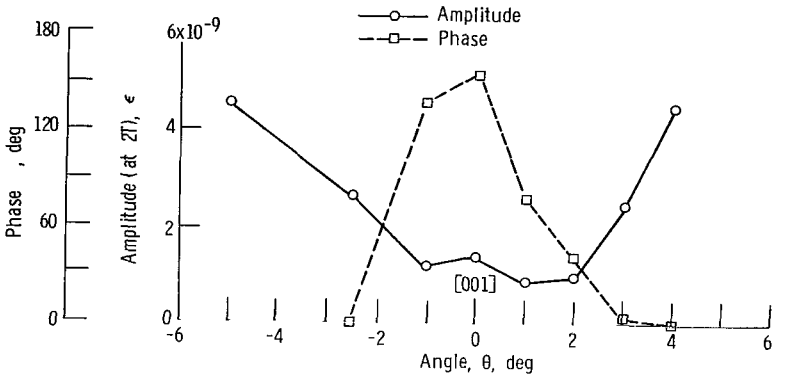

Figure 5. - Amplitude and phase of [110] magnetostriction oscillations for $\vec{B}$ near [001] for sample X6.

The ME amplitude analysis is quite similar to the MS analysis. A linear least squares fit was made of $x = \ln\left[\Delta(Y_{\ell mn})^{-1} B^{1/2} \sinh(\alpha \mu T/B)\right]$ against B^{-1}. From equations (17) and (42) it follows that the Dingle temperature comes from the slope of the curve and that the x intercept gives a value for

$$\cos\left(\frac{\pi g \mu}{2}\right) \sum_{S_m^o} \left[\sum_{i,j=1}^{6} \frac{\partial \epsilon_{\ell mn}}{\partial \epsilon_i} s_{ij}^o \frac{\partial \ln S_m^o}{\partial \epsilon_j} \right]^2$$

The Dingle temperatures found from the ME amplitude analysis are presented in table VII. The ME Dingle temperatures for $\vec{B} \| \langle 110 \rangle$ are consistently lower than the MS Dingle temperatures for the same samples, whereas for $\vec{B} \| \langle 111 \rangle$ the ME Dingle temperatures are larger than the MS Dingle temperatures. This result is unexpected within the framework of our model.

TABLE VII. - DINGLE TEMPERATURE FROM MAGNETOELASTIC OSCILLATIONS

Sample and axis	Field direction					
	$\vec{B}\parallel[100]$	$\vec{B}\parallel[001]$	$\vec{B}\parallel[110]$	$\vec{B}\parallel[\bar{1}10]$	$\vec{B}\parallel[111]$	$\vec{B}\parallel[\bar{1}\bar{1}1]$
	Dingle temperature, K					
X6[100]	9.6±0.8	8.3±1.0	-------	6.8±0.9	--------	-------
X6[110]	-------	8.4±0.4	8.5±0.4	7.5±0.3	--------	8.2±0.5
X6[111]	-------	-------	-------	7.3±0.5	10.2±0.2	-------

Table VIII shows theoretical and experimental values determined for the ME strain derivative sums. The simple theory and full theory values have the same meaning as the MS theoretical values. The elastic constants, deformation potentials and the value of $\cos(\pi g\mu/2)$ used for the theoretical evaluations are the same as those used to calculate the MS amplitude terms. Again, the uncertainty in the theoretical values comes from the uncertainty in $\cos(\pi g\mu/2)$. Recall also that the experimental values depend on the value of K used in the data reduction. Using K = 13 instead of 8.3 leads to a reduction of the experimental values by 17, 19, and 20 percent for the [100], [110], and [111] magnetic field directions, respectively.

Just as we were able to write the MS strain derivative sums in a form that illuminates the signficance of the relative magnitudes of the values in table V, we find that the ME strain derivatuve sums for all the sample and field directions shown in table VII except the case $\epsilon\parallel[110]$ with $\vec{B}\parallel[100]$, can be expressed in the form

$$\sum_{S_m^o} \left[\sum_{i,j=1}^{6} \frac{\partial \epsilon_{lmn}}{\partial \epsilon_i} s_{ij} \frac{\partial \ln S_m^o}{\partial \epsilon_j} \right]^2 = N_e(\beta_d + D\beta_s)^2 \qquad (48)$$

where all the terms have the same meaning as in equation (47). For the case $\epsilon\parallel[110]$ with $\vec{B}\parallel[100]$, the right side of equation (47) becomes $4\left(\beta_d^2 + \frac{1}{4}\beta_s^2\right)$. Remember that, for the comparable MS case, the shear terms β_s cancelled out when summed over the four spheroids. In the ME case, the strain derivatives are all squared before they are summed, and the shear term does not cancel. Since $|\beta_s| >> |\beta_d|$, as seen experi-

TABLE VIII. - EXPERIMENTAL AND THEORETICAL VALUES OF STRAIN DERIVATIVE SUM FROM MAGNETOELASTIC OSCILLATIONS FOR SAMPLE X6

[Theoretical values were computed using $\Xi_m^v = 10.46$ eV.]

Type of data	Sample and axis								
	X6[100]			X6[110]				X6[111]	
	Field direction								
	[100]	[010]	[011]	[110]	$[\bar{1}10]$	[001]	$[\bar{1}\bar{1}1]$	[111]	$[\bar{1}10]$
	Strain derivative sum[a], m^4N^{-2}								
Experimental	$(3.1\pm0.7)\times10^{-18}$	$(2.9\pm0.9)\times10^{-18}$	$(1.3\pm0.3)\times10^{-18}$	$(23\pm3)\times10^{-18}$	$(15\pm2)\times10^{-18}$	$(33\pm4)\times10^{-18}$	$(9.7\pm1.6)\times10^{-18}$	$(2.7\pm0.4)\times10^{-18}$	$(2.6\pm0.3)\times10^{-18}$
Simple theory	0	0	0	(13.5±3)	(13.5±3)	(27±5)	(6.8±1.4)	(27±5)	(6±1)
Full theory	0	0	0	(18.9±4)	(19.3±4)	(37±7)	(9.8±2.0)	(38.5±8)	(8.6±1.7)

[a]Strain derivative sum $= \left| \cos(\pi g\mu/2) \right| \sum_{S_m^o} \left[\sum_{i,j=1}^{6} (\partial \epsilon_{l\,mn}/\partial \epsilon_i) s_{ij}^o (\partial \ln S_m^o/\partial \epsilon_j) \right]^2$.

mentally and theoretically from both the MS and ME data, the MS strain derivative sum for the case $\epsilon \| [110]$ with $\vec{B} \| [100]$ was an order of magnitude less than the sums involving β_s. In contrast, the ME strain derivative sum for this orientation is of the same magnitude as in the other cases.

Using $|\beta_s| >> |\beta_d|$, equation (48) predicts that for X6[110] the ratio of the strain derivative sums for $\vec{B} \| [110]$, [110], [001], and [111], respectively, should be 2:2:4:1 (table VIII). The experimental values confirm this aspect of the theoretical model reasonably well. The experimental values for X6[110] are also in reasonably good agreement with those predicted by the theoretical model. The fact that the ME theoretical values predicted for X6[100] are much smaller than the values measured is not too surprising since our model and calculations contain several simplifying assumptions. The X6[100] experimental values are, in fact, an order of magnitude smaller than the X6[110] experimental values. This we understand qualitatively within the framework of our model. The order of magnitude disagreement between experiment and theory for X6[111] is not understood at this time. The experiments on X6[111] were carefully repeated in an unsuccessful attempt to resolve this discrepancy. Equation (48) predicts that the strain derivative sum for X6[111] with $\vec{B} \| [111]$ should be equal to the X6[110] value for $\vec{B} \| [001]$ and that the value for the X6[111] case with $\vec{B} \| [110]$ should be 2/9 of this value. The MS data for X6[111] gave good agreement between experiment and theory, so the discrepancy does not seem to be associated with this particular sample.

We have already pointed out that the expression for the ratio of the ME to the MS amplitudes is greatly simplified because of the cancellation of most of the coefficient A_{10} which contains, among other things as factors, K and $\cos(\pi g \mu / 2)$. From equations (41), (42), (47), and (48), we see that, for all the sample configurations in tables V and VII except the case $\epsilon \| [110]$ with $\vec{B} \| [001]$, the expression for the ratio of the amplitudes takes the form

$$\frac{\Delta(Y_{l\,mn})^{-1}}{\epsilon_{l\,mn}} = \frac{cS_m^o}{e\hbar B} \sum_{S_m^o} \sum_{i,j=1}^{6} \frac{\partial \epsilon_{l\,mn}}{\partial \epsilon_i} s_{ij}^o \frac{\partial \ln S_m^o}{\partial \epsilon_j} \exp\left[\alpha\mu \frac{\left(T_D^{\epsilon} - T_D^{Y}\right)}{B}\right] \qquad (49)$$

If the Dingle temperatures were the same the right side of equation (49) would have a simple B^{-1} field dependence. The experimentally observed field dependence does, in fact, deviate from B^{-1} and we attribute this wholly to the difference in Dingle temperatures.

Because the X6[100] amplitudes are too small and the X6[111] ME data are questionable, we have only the data from X6[110] for the ratio. (No ME measurements were made on the X5 samples.) By least-squares fitting a semilogarithmic plot of equation (49) for the data from X6[110], we find the parameters presented in tablex IX and X. As can readily be seen from table IX, the ME and MS Dingle temperature difference determined from the ratio (eq. (49)) and the difference obtained from the values from the two separate experiments agree. The nature of this difference is not understood within the framework of our thermodynamic model.

The strain derivative sums determined from the ratio are displayed in table X. The terms simple theory and full theory have the same meanings as above. The experimental values for the ratio are independent of the K value and the $\cos(\pi g\mu/2)$ so that uncertainties in these parameters have no effect on the results. The uncertainties of the experimental values in table X are mainly due to the random uncertainties of the amplitude measurements themselves.

From our theoretical model (see, for instance, table VI and eq. (38)) we find that the strain derivative sums shown in table X are essentially linearly proportional to Ξ_u^V; therefore, for the theoretical values in table X we have scaled the deformation potential to give the best fit of the theory to the experiment. The best value $\Xi_u^V = 7.9 \pm 1.3$ electron volts closely agrees with the 8.5-electron-volt value found from piezoresistance measurements by Burke (ref. 51). When we scale the ME data for a best fit between experiment and theory, we find $\Xi_u^V = 10.1 \pm 1.2$ electron volts. The uncertainty in the deformation potential determined from the ME data comes mainly from the uncertainty in $\cos(\pi g\mu/2)$. For the ME case, however, we must concern ourselves with the question of whether K is 13 or 8.3. The 10-percent uncertainty introduced by this difference is not included in the ±1.2 electron volts.

TABLE IX. - THE DIFFERENCE BETWEEN MAGNETOSTRICTION AND MAGNETOELASTIC DINGLE TEMPERATURES FOR X6[110]

Values from -	Field direction		
	[110]	$[1\bar{1}0]$	$[\bar{1}\bar{1}1]$
	Dingle temperature difference, $T_D^\epsilon - T_D^V$, K		
Eq. (49)[a]	1.4±0.1	1.3±0.7	-1.2±0.2
Tables IV and VII[b]	.7±0.6	.8±0.6	-1.0±0.6

[a]Fitting the ME-MS ratio data to eq. (49).

[b]The difference between the values determined by the two separate experiments.

TABLE X. - STRAIN DERIVATIVE SUM DETERMINED FROM MAGNETOSTRICTION-MAGNETOELASTIC AMPLITUDE RATIO FOR X6[110]

[Theoretical values computed using $\Xi_m^V = 10.46$ eV.]

Type of data	Field direction		
	[110]	$[\bar{1}10]$	$[\bar{1}\bar{1}1]$
	Strain derivative sum[a], m^2N^{-1}		
Experimental	$(37\pm2)\times10^{-10}$	$(26\pm5)\times10^{-10}$	$(48\pm3)\times10^{-10}$
Simple theory	$(31\pm5)\times10^{-10}$	$(31\pm5)\times10^{-10}$	$(31\pm5)\times10^{-10}$
Full theory	$(37\pm6)\times10^{-10}$	$(37\pm6)\times10^{-10}$	$(37\pm6)\times10^{-10}$

[a]Strain derivative sum = $\left| \sum_{S_m^o} \sum_{i,j=1}^{6} (\partial \epsilon_{l\,mn}/\partial \epsilon_i) s_{ij}^o (\partial \ln S_m^o/\partial \epsilon_j) \right|$.

TABLE XI. - SPIN SPLITTING FACTOR (ABSOLUTE VALUE) DETERMINED FROM MAGNETOSTRICTION AND MAGNETOELASTIC AMPLITUDE DATA

[$\Xi_u^V = 7.9\pm1.3$ eV.]

	Sample and strain direction	Field direction				
		[110]	$[\bar{1}10]$	[001]	$[\bar{1}\bar{1}1]$	[111]
		Spin splitting factor, $\lvert\cos(\pi g\mu/2)\rvert$				
Magneto-striction	X5[110]	0.18±0.03	0.17±0.03	---	0.18±0.04	---
	X6[110]	.68±0.13	.76±0.18	---	.59±0.10	---
	X6[111]	---	.44±0.10	---	---	0.52±0.10
Magneto-elastic	X6[110]	0.86±0.33	0.55±0.21	0.63±0.24	0.70±0.28	---

Having found a value for the deformation potential from the MS-ME amplitude ratio we next return to the MS and ME data to find a value for $\cos(\pi g\mu/2)$. Taking $\Xi_u^v = 7.9\pm1.3$ electron volts, we use our theoretical model to compute values for the strain derivative sums and then combine these results with equations (41) and (42) and the experimental amplitudes to find $\cos(\pi g\mu/2)$. The results of this procedure are given in table XI. The comparison of the spin factor found in this manner with the value found directly from the splitting of the oscillation peaks is a further test of the internal consistency of the theoretical model. Assuming $\cos(\pi g\mu/2)$ to be the same in the [100], [110], and [111] directions, and incorporating our phase results, which indicate that this function must be negative, the average of the X5 values in table XI give $\cos(\pi g\mu/2) = -(0.18\pm0.02)$ compared with the spinsplitting value of $-(0.19\pm0.10)$. The X6 values average to $-(0.57\pm0.06)$ compared with the spin splitting value of $-(0.40\pm0.08)$. For this analysis we have used our own values for K. If we had used the K value of Burke, Houston, and Savage (ref. 40) the X5 and X6 data in table XI would have to be shifted down by 28 and 15 percent, respectively. If our model is correct, this indicates that a value of $K = 13$ for $p = 3\times10^{18}$ is too high.

CONCLUSIONS

A detailed experimental and theoretical study of quantum oscillations in the magnetostriction (oscillatory magnetostriction) and Young's modulus (magnetoelastic oscillations) of p-type lead telluride has been presented. The Young's modulus oscillations represents the first observation of quantum oscillations in the elastic constants of a semiconductor. In the theory, the oscillatory magnetostriction and magnetoelastic oscillations are related to strain derivatives of extremal Fermi surface cross-sectional areas using appropriate thermodynamic derivatives of the modified Lifshitz-Kosevich expression for the quantum oscillatory electronic free energy. These strain derivatives are, in turn, related to a deformation potential description of the strain dependence of the electronic band structure using an adaptation of Cohen's nonellipsoidal, nonparabolic band model to describe the nearly spheroidal nonparabolic valence band of lead telluride.

From the periods, phases, and spin splitting of the oscillations, we find experimental band parameters for p-type lead telluride that are in generally good agreement with parameters reported by other workers, although there is a discrepancy with recent results of Burke, Houston, and Savage (ref. 32) and of Schilz (ref. 37) in the value of the Fermi surface anisotropy constant K. These workers found values of K near 13 for carrier concentrations near 3×10^{18} per cubic centimeter, whereas we found $K = 6.5$ for $p = 3.5\times10^{18}$ per cubic centimeter.

The absolute amplitudes of the magnetostriction and magnetoelastic oscillations were were generally in good agreement with the predictions of our theory. From the ratio of the amplitudes of the two types of oscillation, we have derived a value of the valance-band deformation potential $\Xi_u^v = 7.9 \pm 1.3$ electron volts. This agrees well with a value previously obtained by Burke (ref. 16) from piezoresistance measurements. The relative phase of the two types of oscillation is in accord with that predicted by the theory. A detailed study of the absolute amplitudes of the two types of oscillation indicates that the dominant effect of strain on the valance band is a lifting of the degeneracy of the valence band maxima by shear strains accompanied by intervalley charge transfer. The effects of strain on the band parameters (the so-called strain-mass effects) are roughtly an order of magnitude smaller than the intervalley charge transfer effects. This is in contradiction with a conclusion of reference 16 based on oscillatory magnetostriction experiments only. In that analysis these workers used band parameters from the literature that give a value of the spin-splitting factor in disagreement with our experimental observations, and, in addition, their analysis appears to contain a numerical error. If these two features of their analysis are corrected, their results are consistent with small strain-mass effects. Study of our amplitude results also suggests that our value of the Fermi surface anisotropy constant is more nearly correct than the higher values reported by Burke, Houston, and Savage (ref. 37) and by Schilz (ref. 32).

Lewis Research Center,
National Aeronautics and Space Administration,
Cleveland, Ohio, October 6, 1971,
112-27.

APPENDIX - SOME BASIC RELATIONS

In this appendix we present some basic relations between the band parameters for our spheroidal, nonparabolic energy band model of PbTe. Most of the relations follow directly from geometric considerations.

The four $\langle 111 \rangle$ spheroidal bands described by equations (3), (5), and (7) can accommodate a total carrier density p if the volume V_p in momentum space of each spheroid is

$$V_p(E_F) = \left(\frac{p}{8}\right)h^3 = \frac{4}{3}\pi 2m_t E_F (2m_\ell E_F)^{1/2}$$

This requires that the Fermi energy E_F be

$$E_F = \frac{\hbar^2\left(\frac{3\pi^2 p}{4}\right)^{2/3}}{2m_t K^{1/3}} \tag{A1}$$

From straightforward geometrical considerations, the area of intersection S between a plane perpendicular to an axis p_B and a spheroidal Fermi surface is found to be

$$S(\theta, p_B) = \frac{2\pi m_t \sqrt{K}\, E_F}{\left(K\cos^2\theta + \sin^2\theta\right)^{1/2}} - \frac{\pi p_B^2 \sqrt{K}}{\left(K\cos^2\theta + \sin^2\theta\right)^{3/2}} \tag{A2}$$

where θ is the angle between the p_B axis and the spheroid axis and p_B is the distance from the plane to the center of the spheroid.

The period of the quantum oscillations is determined by the maximum cross-sectional area S_m of the Fermi surface perpendicular to the field direction, $p = eh/(cS_m)$. From equation (A2) we see that the maximum cross-sectional area occurs when $p_B = 0$, giving

$$P(\theta) = \frac{e\hbar\left(K\cos^2\theta + \sin^2\theta\right)^{1/2}}{cm_t \sqrt{K}\, E_F} \tag{A3}$$

From equation (A2) we can evaluate one of the important amplitude factors of the Lifshitz-Kosevich equation (eq. (17)):

$$\left|\frac{\partial^2 S}{\partial p_B^2}\right|^{-1/2}_{S=S_m} = \left(\frac{K}{2\pi}\right)^{1/2} \left(\cos^2\theta + \frac{\sin^2\theta}{K}\right)^{3/4} \tag{A4}$$

It is convenient to define a band mass m^* for the nonparabolic bands by the relation

$$\left(\frac{1}{m^*}\right)^2 \equiv \frac{\cos^2\theta}{m_t^2} + \frac{\sin^2\theta}{m_t m_l} \tag{A5}$$

The preceding expressions can be written more easily in terms of this band mass:

$$S_m(\theta) = 2\pi m^* E_F \tag{A6}$$

$$P(\theta) = \frac{e\hbar}{cE_F m^*} \tag{A7}$$

$$\left|\frac{\partial^2 S}{\partial p_B^2}\right|^{-1/2}_{S=S_m} = \left(\frac{K}{2\pi}\right)^{1/2} \left(\frac{m_t}{m^*}\right)^{3/2} \tag{A8}$$

The reduced cyclotron mass for a magnetic field in the B-direction is defined as $\mu = (1/2\pi m_o)\left(\partial S_m/\partial E\right)_{E_F}$. Substituting equation (7) into equation (A2) and differentiating result in

$$\left(\frac{1}{\mu}\right)^2 = \left(\frac{\cos^2\theta}{\mu_t^2} + \frac{\sin^2\theta}{\mu_t \mu_l}\right) \Phi \tag{A9}$$

where

$$\mu_t = \left(\frac{m_1}{m_o}\right)\left(1 + \frac{2E_F}{E_g}\right)$$

$$\mu_l = \frac{m_3}{m_o}$$

and

$$\Phi = (1 - \xi)(1 + 2r)^2(1 + 2r - r\omega)^{-2}$$

and where

$$r \equiv \frac{E_F}{E_g}$$

$$\omega = \frac{1}{2}(1 + r)\left(1 + r + \frac{m_3}{m_1}\cot^2\theta\right)^{-1}$$

and

$$\xi = r\left(1 + 2r + \frac{m_3}{m_1}\cot^2\theta\right)^{-1}$$

Using the experimental results for PbTe Φ is found to be very near 1 when the field is in any of the principal crystallographic directions: For the X6 samples $0.99 < \Phi < 1$, and, for X5, $0.97 < \Phi < 1$. Thus, for all practical purposes we can set $\Phi = 1$. Notice that $\mu_t \neq m_t/m_o$, except for $E_F/E_g = 0$.

REFERENCES

1. Gold, A. V.: The de Haas-van Alphen Effect. Solid State Physics. Vol. 1. Electrons in Metals. J. F. Cochran and R. R. Haering, eds., Gordon and Breach Science Publ., 1968, pp. 39-126.

2. Lifshitz, I. M.; and Kosevich, A. M.: Theory of Magnetic Susceptibility in Metals at Low Temperatures. Soviet Phys.-JETP, vol. 2, no. 4, July 1956, pp. 636-645.

3. Joule, J. P.: On a New Class of Magnetic Forces. Annals of Electricity. Vol. 8, 1842, p. 219.

4. Kapitza, P.: Magnetostriction of Diamagnetic Substances in Strong Magnetic Fields. Nature, vol. 124, 1929, p. 53. (See also Kapitza, P: The Study of the Magnetic Properties of Matter in Strong Magnetic Fields. Part III - Magnetostriction. Proc. Roy. Soc. (London), Ser. A, vol. 135, no. 828, Apr.1, 1932, pp. 537-555.)

5. Chandrasekhar, B. S.: A Note on the Possibility of Observing deHaas-van Alphen Oscillations in Magnetostriction. Phys. Letters, vol. 6, no. 1, Aug. 15, 1963, pp. 27-28.

6. Green, Ben A., Jr.; and Chandrasekhar, B. S.: Observation of Oscillatory Magnetostriction in Bismuth at 4.2° K. Phys. Rev. Letters, vol. 11, no. 7, Oct. 1, 1963, pp. 331-332.

7. Aron, Paul R.: Oscillatory Magnetostriction of Silver and Copper. Bull. Am. Phys. Soc., vol. 15, no. 3, Mar. 1970, pp. 263-264.

8. Thompson, T. E.: Oscillatory Magnetostriction of Arsenic. Bull. Am Phys. Soc., vol. 15, no. 3, Mar. 1970, p. 264.

9. Chandrasekhar, B. S.; Fawcett, E.; Sparlin, D. M.; and White, G. K.: Oscillatory Magnetostriction in Beryllium. Proceedings of the 10th International Conference on Low Temperature, Vol. 3. M. P. Malkov, ed., Proizvod-strenno-Izdatel'skii Kombinat, VINITI, Moscow, 1967, p. 328.

10. Aron, P.R.; and Chandrasekhar, B. S.: Oscillatory Magnetostriction and Deformation Potentials in Bismuth. Phys. Letters, vol. 30A, no. 2, Sept. 22, 1969, pp. 86-87.

11. Sparlin, Don M.; and Carter, James M.: Monotonic Magnetostriction in Cadmium. Bull. Am. Phys. Soc., vol. 15, no. 3, Mar. 1970, p. 270.

12. Fawcett, E.: Oscillatory Magnetostriction in Antiferromagnetic Chromium. Bull. Am. Phys. Soc., vol. 15, no. 3, Mar. 1970, p. 264.

13. Slavin, A. J.: Oscillatory Magnetostriction of Copper and Tin and Monotonic Magnetostriction of Zirconium. M. S. Thesis, Univ. Toronto, 1968.

14. Chandrasekhar, B. S.; Condon, J. H.; Fawcett, E.; and Becker, W. M.: Oscillatory Magnetostriction in n-Gallium Antimonide. Phys. Rev. Letters, vol. 17, no. 18, Oct. 31, 1966, pp. 954-955.

15. Aron, P. R.; Chandrasekhar, B. S.; and Thompson, T. E.: Oscillatory Magnetostriction in p-Type PbTe. Presented at the Am. Phys. Soc. Meeting, Chicago, Ill., 1967.

16. Belson, Henry S.; Burke, J. Richard; Callen, Earl; Houston, Bland; Savage, Howard T.; Babiskin, J.; and Siebenmann, P. G.: Oscillatory Magnetostriction in p-Type PbTe. Phys. Rev. Letters, vol. 19, no. 25, Dec. 18, 1967, pp. 1428-1431.

17. Mahajan, V. N.; and Sparlin, D. M.: Magnetostriction in Antimony. Bull. Am. Phys. Soc., vol. 12, no. 3, Mar. 1967, p. 286.

18. Reitz, L.; and Sparlin, D. M.: Oscillatory Magnetostriction in Zinc. Bull. Am. Phys. Soc. vol. 11, no. 2, Feb. 1966, p. 169.

19. Nye, John F.: Physical Properties of Crystals: Their Representation by Tensors and Matrices. Clarendon Press, Oxford, 1957, Ch. 8, p. 34.

20. Thompson, T. E.; and Langenberg, D. N.: Magnetoelastic Quantum Oscillations in PbTe. Solid State Commun., vol. 8, no. 19, Oct. 1, 1970, pp. 1503-1508.

21. Mavroides, J. G.; Lax, B.; Button, K. J.; and Shapira, Y.: Oscillatory Quantum Effects in the Ultrasonic Velocity in Bismuth. Phys. Rev. Letters, vol. 9, no. 11, Dec. 1, 1962, pp. 451-453.

22. Quinn, John J.; and Rodriguez, Sergio: Magnetic-Field Dependence of the Velocity of Sound in Metals. Phys. Rev. Letters, vol. 9, no. 4, Aug. 15, 1962, pp. 145-147.

23. Rodriguez, Sergio: Oscillations of the Velocity of Sound in Metals in a Magnetic Field. Phys. Rev., vol. 132, no. 2, Oct. 15, 1963, pp. 535-541.

24. Testardi, L. R.; and Condon, J. H.: Landau Quantum Oscillations of the Velocity of Sound in Be: The Strain Dependence of the Fermi Surface. Phys. Rev., vol. 1B, no. 10, May 15, 1970, pp. 3928-3942.

25. Lin, P. J.; and Kleinman, L.: Energy Bands of PbTe, PbSe, and PbS. Phys. Rev., vol. 142, no. 2, Feb. 11, 1966, pp. 478-489.

26. Cuff, K. F.; Ellett, M. R.; and Kuglin, C. D.: Band Structure and Transport Properties of PbTe. Proceedings of the International Conference Physics of Semiconductors. A. C. Strickland, ed., Inst. Physic and Phys. Soc., London, 1962, p. 316-322.

27. Cuff, K. F.; Ellett, M. R.; Kuglin, C. D.; and Williams, L. R.: The Band Structure of PbTe, PbSe, and PbS. Proceedings of the 7th International Conference on the Physics of Semiconductors. Michel Hulin, ed., Academic Press, 1964, pp. 677-684.

28. Dixon, Jack R.; and Riedl, H. R.: Electric-Susceptibility Hole Mass of Lead Telluride. Phys. Rev., vol. 138A, no. 3, May 3, 1965, pp. 873-881.

29. Kane, Evan O.: Band Structure of Indium Antimonide. J. Phys. Chem. Solids, vol. 1, no. 4, 1957, pp. 249-261.

30. Cohen, Morrel H.: Energy Bands in the Bismuth Structure. I. A Nonellipsoidal Model for Electrons in Bi. Phys. Rev., vol. 121, no. 2, Jan. 15, pp. 387-395.

31. Cuff, K. F.; Ellett, M. R.; and Kuglin, C. D.: Oscillatory Magnetoresistance in the Conduction Band of PbTe. J. Appl. Phys., vol. 32, no. 10, Suppl., Oct. 1961, pp. 2179-2185.

32. Schilz, W.: Magneto-Acoustic Investigation of the Fermi Surface and Spin Splitting of the Landau Levels in p-Type and n-Type PbTe. J. Phys. Chem. Solids, vol. 30, Apr. 1969, pp. 893-901.

33. Mitchell, D. L.: Palik, E. D.; and Zemel, J. N.: Magneto-Optical Band Studies of Epitaxial PbS, PbSe and PbTe. Proceedings of the 7th International Conference on the Physics of Semiconductors. Michel Hulin, ed., Academic Press, 1964, pp. 325-333.

34. Butler, J. F.; and Calawa, A. R.: Magnetoemission Studies of PbS, PbTe, and PbSe Diode Lasers. Physics of Quantum Electronics. P. L. Kelley, B. Lax, and P. E. Tannenwald, eds., McGraw-Hill Book Co., Inc., 1966, pp. 458-466.

35. Roth, Laura M.: g-Factor and Donor Spin-Lattice Relaxation for Electrons in Germanium and Silicon. Phys. Rev., vol. 118, no. 6, June 15, 1960, pp. 1534-1540.

36. Cohen, M. H.; and Blount, E. I.: The g-factor and de Haas-van Alphen Effect of Electrons in Bismuth. Phil. Mag., vol. 5, no. 50, Feb. 1960, pp. 115-126.

37. Burke, J. Richard; Houston, Bland; and Savage, H. T.: Anisotropy of the Fermi Surface of p-Type PbTe. Phys. Rev., vol. 2B, no. 6, Sept. 15, 1970, pp. 1977-1988.

38. Bardeen, J.; and Shockley, W.: Deformation Potentials and Mobilities in Non-polar Crystals. Phys. Rev., vol. 80, no. 1, Oct. 1, 1950, pp. 72-80.

39. Herring, C.: Transport Properties of a Many-Valley Semiconductor. Bell Sys. Tech. J., vol. 34, no. 2, Mar. 1955, pp. 237-290.

40. Herring, Conyers; and Vogt, Erich: Transport and Deformation-Potential Theory for Many-Valley Semiconductors with Anisotropic Scattering. Phys. Rev., vol. 101, no. 3, Feb. 1, 1956, pp. 944-961.

41. Ferreira, Luiz G.: Deformation Potentials of Lead Telluride. Phys. Rev., vol. 137A, no. 5, Mar. 1, 1965, pp. 1601-1609.

42. Ilisavskii, Yu V.: Piezoresistance Effect in PbTe and PbSe. Soviet Phys.-Solid State, vol. 4, no. 4, Oct. 1962, pp. 674-680.

43. Burke, J. Richard, Jr.: Piezoresistance Effect in p-Type PbTe. Phys. Rev., vol. 160, no. 3, Aug. 15, 1967, pp. 636-648.

44. Forgacs, R. L.: Improved Sing Around System for Ultrasonic Velocity Measurements. IRE Trans on Instrumentation, vol. I-9, no. 3, Dec. 1960, pp. 359-367.

45. Condon, J. H.: Nonlinear de Haas-van Alphen Effect and Magnetic Domains in Beryllium. Phys. Rev., vol. 145, no. 2, May 13, 1966, pp. 526-535.

46. Williamson, S. J.; Foner, S.; and Smith, R. A.: Influence of Landau Level Broadening on the de Haas-van Alphen Effect. Phys. Rev., vol. 136A, no. 4, Nov. 16, 1965, pp. 1065-1067.

47. White, G. K.: Measurement of Thermal Expansion at Low Temperatures. Cryogenics, vol. 1, no. 3, Mar. 1961, pp. 151-158.

48. Quimby, S. L.: On the Experimental Determination of the Viscosity of Vibrating Solids. Phys. Rev., vol. 25, Apr. 1925, pp. 558-573.

49. Balamuth, L.: A New Method for Measuring Elastic Moduli and the Variation with Temperature of the Principal Young's Modulus of Rocksalt Between 78° K and 273° K. Phys. Rev., vol. 45, May 15, 1934, pp. 715-720.

50. Thompson, Thomas E.: Oscillatory Magnetostriction and Magnetoelastic Oscillations in p-Type Lead Telluride. Ph. D. Thesis, Univ. of Pennsylvania, 1969.

51. Stiles, P. J.; Burstein, E.; and Langenberg, D. N.: Azbel-Kaner Cyclotron Resonance in p-Type PbTe. Phys. Rev. Letters, vol. 9, no. 6, Sept. 15, 1962, pp. 257-259.

52. Stiles, P. J.; Burstein, E.; and Langenberg, D. N.: de Haas-van Alphen Effect in p-Type PbTe and n-Type PbS. J. Appl. Phys., vol. 32, no. 10, Suppl., Oct. 1961, 2174-2178.

53. Coste, G.: Oscillatory Thermomagnetic Effects in Lead Telluride. Phys. Stat. Sol., vol. 20, 1967, pp. 361-364.

54. Patel, C. K. N.; and Slusher, R. E.: Electron Spin-Flip Raman Scattering in PbTe. Phys. Rev., vol. 177, no. 3, Jan. 15, 1969, pp. 1200-1202.

55. Houston, Bland; Strakna, R. E.; and Belson, Henry S.: Elastic Constants, Thermal Expansion, and Debye Temperature of Lead Telluride. J. Appl. Phys., vol. 39, no. 8, July 1968, pp. 3913-3916.

NASA-Langley, 1972 —— 26 E-6524

"The aeronautical and space activities of the United States shall be conducted so as to contribute . . . to the expansion of human knowledge of phenomena in the atmosphere and space. The Administration shall provide for the widest practicable and appropriate dissemination of information concerning its activities and the results thereof."

—NATIONAL AERONAUTICS AND SPACE ACT OF 1958

NASA SCIENTIFIC AND TECHNICAL PUBLICATIONS

TECHNICAL REPORTS: Scientific and technical information considered important, complete, and a lasting contribution to existing knowledge.

TECHNICAL NOTES: Information less broad in scope but nevertheless of importance as a contribution to existing knowledge.

TECHNICAL MEMORANDUMS: Information receiving limited distribution because of preliminary data, security classification, or other reasons.

CONTRACTOR REPORTS: Scientific and technical information generated under a NASA contract or grant and considered an important contribution to existing knowledge.

TECHNICAL TRANSLATIONS: Information published in a foreign language considered to merit NASA distribution in English.

SPECIAL PUBLICATIONS: Information derived from or of value to NASA activities. Publications include conference proceedings, monographs, data compilations, handbooks, sourcebooks, and special bibliographies.

TECHNOLOGY UTILIZATION PUBLICATIONS: Information on technology used by NASA that may be of particular interest in commercial and other non-aerospace applications. Publications include Tech Briefs, Technology Utilization Reports and Technology Surveys.

Details on the availability of these publications may be obtained from:

SCIENTIFIC AND TECHNICAL INFORMATION OFFICE

NATIONAL AERONAUTICS AND SPACE ADMINISTRATION

Washington, D.C. 20546